Xcr1^{+} type 1 conventional dendritic cells are essential mediators for atherosclerosis progression

Running tittle: Targeting of cDC1 cells attenuates atherosclerosis

Tianhan Li[1#], Liaoxun Lu[2#], Juanjuan Qiu[2], Xin Dong[2], Le Yang[2], Kexin He[2], Yanrong Gu[2], Binhui Zhou[2], Tingting Jia[2], Toby Lawrence[3], Marie Malissen[3], Guixue Wang[4], Rong Huang[2], Hui Wang[2], Bernard Malissen[3*], Yinming Liang[2,5*] Lichen Zhang[2*]

[1]*School of Basic Medicine, Xinxiang Medical University, Xinxiang, China.*

[2]*School of Medical Technology, Xinxiang Medical University, Xinxiang, China.*

[3]*Centre d'Immunologie de Marseille-Luminy, INSERM, CNRS, Aix-Marseille Université, Marseille, France*

[4]*Key Laboratory for Biorheological Science and Technology of Ministry of Education, State and Local Joint Engineering Laboratory for Vascular Implants, Bioengineering College of Chongqing University, Chongqing, China*

[5]*Center of Disease Model and Immunology, Hunan Academy of Chinese Medicine, Changsha, China.*

[#]*These authors contributed equally to this work.*

[*]Correspondence: yinming.liang@gris.org.cn (Y L); zhanglichen@gris.org.cn (L Z). bernardm@ciml.univ-mrs.fr (B M).

Abstract:

Background:

Atherosclerosis is characterized by lipid accumulation within plaques, leading to foam cell

formation and an inflammatory response within the aortic lesions. Lipid disorders have been extensively investigated, however the cellular and molecular mechanisms that trigger the inflammatory response in atherosclerotic plaques remain far from being fully understood. Xcr1^{+} cDC1 cells are newly identified antigen-presenting cells in activating immune cells. However, the role of cDC1 cells in the development of atherosclerosis remains highly controversial.

Methods and Results:

We first confirmed the presence of cDC1 within human atherosclerotic plaques and discovered a significant association between the increasing cDC1 numbers and atherosclerosis progression in mice. Subsequently, we established Xcr1$^{Cre\text{-}Gfp}$ Rosa26$^{LSL\text{-}DTA}$ ApoE$^{-/-}$ mice, a novel and complex genetic model, in which cDC1 was selectively depleted in vivo during atherosclerosis development. Intriguingly, we observed a notable reduction in atherosclerotic lesions in hyperlipidemic mice, alongside suppressed T cell activation of both CD4^{+} and CD8^{+} subsets in the aortic plaques. Notably, aortic macrophages and serum lipid levels were not significantly changed in the cDC1-depleted mice. Single-cell RNA sequencing revealed heterogeneity of Xcr1^{+} cDC1 cells across the aorta and lymphoid organs under hyperlipidemic conditions. As Xcr1 is the sole receptor for Xcl1, we next explored to target Xcr1^{+} cDC1 cells via Xcl1 by establishing Xcl1 and ApoE deficient mice. Our data indicate that atherosclerotic lesions mediated by cDC1 are dependent on Xcl1.

Conclusions:

Our results reveal crucial roles of cDC1 in atherosclerosis progression and provide insights into the development of immunotherapies by targeting cDC1 through Xcl1.

Introduction

Atherosclerosis is a chronic inflammatory disease that affects the large and medium-sized arteries, and it is the leading cause of cardiovascular mortality and morbidity worldwide [1]. Atherosclerosis is a complex pathological process during which lipid-laden phagocytes such as macrophages, along with lymphocytes and dendritic cells, accumulate in the plaque [2]. Mounting evidence from animal models and human studies demonstrates involvement of both the innate and adaptive immunity in the development of atherosclerosis [3-5]. In healthy arteries, DCs are typically present in the subendothelial space and work in the front line of immune surveillance [6, 7], and small portion of resident vascular DCs are localized in the adventitia. Various studies have demonstrated that DCs accumulated in the advanced atherosclerotic lesions in both humans and animal models [8-11]. Recently, several phenotypically and functionally distinct vascular DCs have been identified in mouse and human atherosclerotic lesions [12]. Xcr1^{+} type 1 conventional dendritic cells (Xcr1^{+} cDC1) (also known as CD8^{+} DC or CD103^{+} DCs) has been recognized for its role in cross-presentation and activating naive CD8^{+} T cells, and are critical for anti-viral and anti-tumor immune responses [13, 14]. Owing to the challenges associated with obtaining a model for specific cDC1 depletion *in vivo*, previous studies investigating the role of cDC1 cells in atherosclerosis using various knockout mice have produced conflicting results [15-19]. It is important to note that previous Cre lines developed to achieve specific Cre expression in cDC1s still led to leakiness in recombinase activity outside of cDC1s, as demonstrated in previous publications [20, 21]. Moreover, scant mechanistic understanding regarding the regulation of cDC1 activity during atherosclerosis has been reported. Therefore, developing a more specific mouse model for cDC1 is essential for elucidating its precise role in atherosclerosis. Here, we established a novel Cre line Xcr1$^{Cre\text{-}Gfp}$ mice and did not observe any leakiness of Cre activity, and

further experiments revealed that specific depletion cDC1 attenuates atherosclerosis development by inhibiting both $CD4^+$ and $CD8^+$ T cell activation in hyperlipidemic $Xcr1^{Cre\text{-}Gfp}$ $Rosa26^{LSL\text{-}DTA}$ $ApoE^{-/-}$ mice.

The origin of phagocytes within the atherosclerotic plaques has been controversial. Studies have shown that the major contribution of macrophages in the aortic plaque is recruited from the circulation, while other studies have emphasized the significance of local proliferation [22, 23]. Tissue-resident dendritic cells inside the plaques have been well documented [24, 25], regardless of the fact that the contribution and origin of $Xcr1^+$ cDC1 have not been appropriately addressed. To understand the origin of $Xcr1^+$ cDC1 inside the plaque, we performed bone marrow transplantation using $Xcr1^{Cre\text{-}Gfp}$ $Rosa26^{LSL\text{-}DTA}$ mice as donors and found that in $ApoE^{-/-}$ recipient mice placed on a high-fat diet (HFD), cDC1 cells were completely absent in the aortas. Therefore, our experiments have elucidated that cDC1 cells in the atherosclerotic plaques originate from the bone marrow. Further single cell RNA sequencing illustrated that notable differences in $Xcr1^+$ cDC1 cells are discovered among the aorta, spleen, and lymph nodes. *Ccr2*, *Sept3* and *Cldnd1* were highly expressed in $Xcr1^+$ cDC1 cells from aorta compared with that from spleen and lymph nodes.

We further aimed to ascertain whether cDC1 can be modulated by targeting the chemokine Xcl1, which is a ligand of Xcr1. Considering the vital role that $Xcr1^+$ cDC1 plays in the progression of atherosclerosis and the therapeutic potential of manipulating their functions via chemokines[26], comprehending the feasibility of targeting Xcl1 holds considerable promise for developing novel therapeutic approaches to halt the advancement of atherosclerosis. We conducted further studies using $Xcl1^{-/-}$ $ApoE^{-/-}$ double knockout mice to assess the pathological grade of atherosclerotic

lesions. Our data indicated that the knockout of Xcl1 led to a mild yet significant reduction of cDC1 cells in the aorta. However, strikingly, when compared to the ApoE$^{-/-}$ control mice, the Xcl1$^{-/-}$ ApoE$^{-/-}$ mice exhibited a markedly decreased severity of the atherosclerotic lesions, to an extent comparable to that observed in cDC1-depleted Xcr1$^{Cre\text{-}Gfp}$ Rosa26$^{LSL\text{-}DTA}$ ApoE$^{-/-}$ mice.

Therefore, our study which employed genetic models to deplete Xcr1^{+} cDC1 *in vivo* in hyperlipidemic mice, has unequivocally determined the essential role of this specific cell type in the development of atherosclerosis. Besides their well-established role in cross-presentation to CD8^{+} T cells, recent studies have shown Xcr1^{+} cDC1 cells also engage with CD4^{+} T cells to augment CD8^{+} T cell responses [20, 27]. Our data showing Xcr1^{+} cDC1-dependent CD4 and CD8 T cell activation in atherosclerotic plaques is in line with the new paradigm for cDC1s as a platform for both CD4 and CD8 T cell responses in the novel context of atherosclerosis.

Most importantly, we have successfully demonstrated that targeting the chemokine Xcl1, the ligand of Xcr1, can effectively inhibit atherosclerosis. These novel findings hold the potential to forge a novel trajectory for therapeutic interventions within the field of atherosclerosis, presenting promising prospects for better understanding and treatment of this disorder.

Results:

Progressive accumulation of Xcr1^{+} cDC1 cells in advanced atherosclerotic lesions in human and mice

Dendritic cells are present in healthy arteries and accumulate within atherosclerotic lesions, participating in various pathogenic and protective mechanisms during atherogenesis [28, 29].

However, the intra-plaque dynamics of cDC1 and their contribution to atherosclerosis remain undetermined. Using the archived specimens of paraffin-embedded human atherosclerotic arteries from our previous study [30], we examined the Xcr1^{+} dendritic cells in human atherosclerotic plaques. As shown in **Figure 1A and 1B**, Xcr1^{+} dendritic cells were significantly more abundant in the plaque area of the human femoral artery compared to that in the plaque-free area. Similarly, the immunofluorescence staining results using specific antibodies for Xcr1 and CD11c revealed that Xcr1^{+}CD11c^{+} dendritic cells accumulated in the plaques of the aortic root in ApoE$^{-/-}$ mice that were placed on a HFD for 16 weeks (**Figure 1C and 1D**). Sample preparations entailed sectioning and appropriate fixation of the aortic root tissues, which were described in greater detail in the Methods and Materials section. To further elucidate the dynamics of Xcr1^{+} cDC1 cells within the plaque during the progression of atherosclerosis, we carried out immunohistochemical analyses of these cells in the lesioned aortic root (**Figure 1E**). The area positive for Xcr1 expression was quantified at 8-week on a chow diet, 8-week on HFD, 12-week on HFD and 16-week on HFD, respectively. Quantitative analysis was conducted using image processing software, revealing a continuous accumulation of Xcr1^{+} cDC1 cells in the lesioned area as the disease progressed (**Figure 1F**). Therefore, our experiments provided data indicating the enrichment of Xcr1^{+} cDC1 cells in aortic lesions in both humans and mice, and demonstrated that the accumulation of Xcr1^{+} cDC1 cells was significantly greater during the progression of atherosclerosis.

Xcr1$^{Cre\text{-}Gfp}$ is selectively expressed in cDC1

To understand the role of Xcr1^{+} cDC1 in regulating the development of atherosclerosis, we established the Xcr1$^{Cre\text{-}Gfp}$ ApoE$^{-/-}$ mice in which the Cre recombinase and eGFP was co-expressed

under the control of endogenous Xcr1 promoter following start codon (**Figure S1**). This new Cre line differs from a previous design in which Cre recombinase was expressed via IRES linkage at the 3' UTR and leaked expression of Cre was frequently observed [20, 31]. To verify the fidelity of Cre expression under hyperlipidemic condition, we used hyperlipidemic ApoE$^{-/-}$ mice as recipient mice and used bone marrow cells from Xcr1$^{Cre\text{-}Gfp}$ Rosa26$^{LSL\text{-}tdRFP}$ mice as donors for the bone marrow transplantation (**Figure 2A**). In Xcr1$^{Cre\text{-}Gfp}$ Rosa26$^{LSL\text{-}tdRFP}$ mice, the presence of Cre protein would turn on the expression of tdRFP as a reporter for the activity of Cre recombinase [32]. Remarkably, we found that the expression of tdRFP was exclusively present in Xcr1^{+} cDC1 when mice were fed a HFD for 16 weeks in the bone marrow transplanted mice, and the Cre recombinase activity was not detectable in non-cDC1 cells (**Figure 2B and 2C**).

To determine the specificity of GFP expression originating from Xcr1$^{Cre\text{-}Gfp}$ genetic modification, we examined the GFP levels in three populations of DCs, namely pDC, cDC1, and cDC2 cells, from the spleen of Xcr1$^{Cre\text{-}Gfp}$ ApoE$^{-/-}$ mice that were fed a HFD for 16 weeks. As expected, we found that the GFP expression was stringently restricted to cDC1 cells (**Figure 2D and 2E**). In parallel, we compared the GFP expression in Xcr1^{+} cDC1-depleted mice that were fed a HFD for 16 weeks. Such cDC1-depleted Xcr1$^{Cre\text{-}Gfp}$ Rosa26$^{LSL\text{-}DTA}$ ApoE$^{-/-}$ mice were obtained by crossing Xcr1$^{Cre\text{-}Gfp}$ ApoE$^{-/-}$ mice with Rosa26$^{LSL\text{-}DTA}$ ApoE$^{-/-}$ mice. Strikingly, we observed a complete loss of GFP-positive cells and Xcr1^{+} cDC1 cells in Xcr1^{+} cDC1-depleted mice (**Figure 2D and 2F**). We also examined DCs, including pDCs, cDC1, and cDC2, in the lymph nodes and spleens of Xcr1$^{Cre\text{-}Gfp}$ Rosa26$^{LSL\text{-}DTA}$ ApoE$^{-/-}$ and ApoE$^{-/-}$ mice maintained on a chow diet for 7 weeks. The flow cytometric analyses also confirmed the absence of Xcr1^{+} cDC1 population in Xcr1$^{Cre\text{-}Gfp}$ Rosa26$^{LSL\text{-}DTA}$ ApoE$^{-/-}$ mice (**Figure S2**). Collectively, these data suggest that Cre recombinase

activity was selectively confined to cDC1 cells, and no leakiness was observed in lineages other than the Xcr1^{+} cDC1 population. We also demonstrated that Xcr1$^{Cre\text{-}Gfp}$ Rosa26$^{LSL\text{-}DTA}$ ApoE$^{-/-}$ mice constitute a desirable model for exploring the role of cDC1 in atherosclerosis.

The specific depletion of Xcr1^{+} cDC1 cells significantly alleviates atherosclerosis without influencing the lipid profile and the number of intra-plaque macrophages

To investigate the role of cDC1 cells in atherosclerosis, both Xcr1$^{Cre\text{-}Gfp}$ Rosa26$^{LSL\text{-}DTA}$ ApoE$^{-/-}$ and the control ApoE$^{-/-}$ mice were subjected to a HFD for 16 weeks. The ORO staining results demonstrated that the size of lesion in both descending aorta and aortic root was significantly smaller in Xcr1$^{Cre\text{-}Gfp}$ Rosa26$^{LSL\text{-}DTA}$ ApoE$^{-/-}$ mice compared with ApoE$^{-/-}$ control mice (12.82% *vs* 6.01% in descending aorta, $p < 0.001$; 39.25% *vs* 33.57% in aortic root, $p < 0.01$) (**Figure 3A-D**). Given that macrophages play a pivotal role in the development and progression of atherosclerotic lesions, particularly within the necrotic core [33, 34], we next investigated macrophage involvement in the aorta using IHC and flow cytometry. Interestingly, no significant differences were observed in the necrotic core area of the aortic root between Xcr1$^{Cre\text{-}Gfp}$ Rosa26$^{LSL\text{-}DTA}$ ApoE$^{-/-}$ mice and ApoE$^{-/-}$ control mice (**Figure 3E and 3F**). Similarly, subsequent flow cytometry analyses and IHC results revealed comparable proportions of F4/80^{+} CD11b^{+} macrophages in the aorta, as well as similar percentages of CD68-positive macrophages in the aortic lesions between the two groups of mice (**Figure 3G-I**). Furthermore, since dyslipidemia is a key characteristic of HFD-treated ApoE$^{-/-}$ mice [35, 36], it is critical to assess body weight and lipid profiles in both groups. Our results indicated no significant differences in body weight or levels of total cholesterol (TC), triglycerides (TG), low-density lipoprotein (LDL), and high-density lipoprotein (HDL) between the two groups (**Figure S3A-B**). Additionally, ORO staining of the liver revealed

no significant differences either (**Figure S3C-D**). Taken together, these results suggested that specific depletion of cDC1 attenuated atherogenesis without affecting lipid status or macrophagic accumulation in aortic lesions.

Specific depletion of cDC1 attenuates the development of atherosclerosis by modulating the activation of T cell in ApoE$^{-/-}$ mice

T cells are among the critical drivers of the pathogenesis of atherosclerosis, and therefore, the triggers of T cell activation in aortic plaques are of great interest for controlling disease progression [2, 37, 38]. We initially analyzed the cDC1 cells through flow cytometry in both Xcr1^{+} cDC1 depleted mice and control mice. In the Xcr1$^{Cre\text{-}Gfp}$ Rosa26$^{LSL\text{-}DTA}$ ApoE$^{-/-}$ mice that were fed a HFD for 16 weeks, we observed a total absence of Xcr1^{+} cDC1 in the aorta, lymph nodes, and spleen (**Figure 4A-B and Figure S4**). Subsequently, we aimed to explore the T cell phenotype in the two groups of mice, and found that the activation of aortic CD4^{+} and CD8^{+} T cells were both significantly inhibited. The expression of CD69 in aortic CD4^{+} and CD8^{+} T cells was significantly lower in the Xcr1^{+} cDC1 depleted mice after being placed on a HFD for 16 weeks (**Figure 4C-D**). Interestingly, such decreased frequencies of CD69^{+} T cells were only observed in aortic lesions but not in lymphoid organs such as lymph nodes and the spleen in the Xcr1^{+} cDC1 depleted mice (**Figure S5A-B and S5D-E**). We further analyzed the absolute numbers of CD8^{+} and CD4^{+} T cells in the spleen and lymph nodes and found that the absolute numbers of CD8^{+} and CD4^{+} T cells were markedly reduced in the spleen but not in the lymph nodes in Xcr1$^{Cre\text{-}Gfp}$ Rosa26$^{LSL\text{-}DTA}$ ApoE$^{-/-}$ mice compared to those in ApoE$^{-/-}$ mice (**Figure S5C and S5F**). Absence of cDC1 also resulted in reduced frequencies of CD8^{+} T cells in both spleen and lymph nodes in hyperlipidemic mice. We also analyzed T cell populations in the lymph nodes

and spleen in two groups of mice that were fed a chow diet and found that the frequencies of $CD8^+$ T cells were significantly decreased in the lymph nodes of $Xcr1^+$ cDC1 depleted mice (**Figure S6A-B**). More importantly, the frequencies of $CD44^{high}$ $CD62L^{low}$ activated memory cells within the $CD8^+$ subsets in both the spleen and lymph nodes were significantly lower than those in the $ApoE^{-/-}$ control mice (**Figure S6A-D**). However, in the $CD4^+$ subsets, such frequencies of $CD44^{high}$ $CD62L^{low}$ activated cells were comparable in the lymph nodes but marginally lower in the spleen (**Figure S6A-D**). It is important to note that the decreased absolute number of $CD8^+$ T cells in the spleen in $Xcr1^+$ cDC1 depleted mice was only observed in HFD groups but not in chow diet groups (**Figure S5F and Figure S6F**). Our data indicate that in aortic plaques, $Xcr1^+$ cDC1 cells are implicated in activating $CD4^+$ and $CD8^+$ T cells, and the loss of the cDC1 population led to a decreased absolute count of $CD8^+$ T cells in the lymph nodes of HFD treated mice. Whereas in mice treated with a chow diet, the loss of the cDC1 population resulted in reduced frequencies of activated memory T cells but did not affect the absolute counts of T cells. Attenuated T cell activation might account for the mitigated atherosclerosis in $Xcr1^+$ cDC1 depleted mice.

Characterization of aortic $Xcr1^+$ cDC1 cells in atherosclerotic lesions

Although the majority of cDC1 cells derive from bone marrow, other mechanisms such as local proliferation of existing DCs can also contribute to the cDC1 population in inflammatory diseases [39, 40]. It remains unclear whether cDC1 cells in lymphoid organs such as spleen and lymph nodes represent a different status compared to cDC1 cells in atherosclerotic lesions. To elucidate the source and status of $Xcr1^+$ cDC1 in atherosclerotic lesions, we performed bone marrow transplantation and single-cell RNA sequencing (sc-RNA seq) of cDC1 cells from aortic plaques

and lymphoid organs. We conducted bone marrow transplantation using Xcr1$^{Cre\text{-}Gfp}$ Rosa26$^{LSL\text{-}DTA}$ or WT mice that carry the CD45.2 congenic markers as donors, and CD45.1^{+} CD45.2^{+} ApoE$^{-/-}$ mice as recipients (**Figure S7A**). Our data showed that body weight, lipid profile, hepatic lipid accumulation were comparable between two groups of bone marrow transplanted mice after being fed with a HFD for 16 weeks (**Figure S7B-D**). Interestingly, flow cytometric analysis of the aorta displayed almost complete depletion of cDC1 cells in ApoE$^{-/-}$ recipient mice transplanted with Xcr1$^{Cre\text{-}Gfp}$ Rosa26$^{LSL\text{-}DTA}$ bone marrow mice (**Figure S7E**). Strikingly we did not find observe significant changes in pDCs and CD64^{+}F4/80^{+} aortic macrophages (**Figure S7E-F**). Therefore, our bone marrow transplantation experiments further confirmed fidelity of the Cre recombinase expression in cDC1 cells in mice.

Next, we carried out sc-RNA seq to characterize Xcr1^{+} cDC1 cells from multiple organs of hyperlipidemic mice. Due to the scarcity of Xcr1^{+} cDC1 cells that can be sorted by FACS and processed for sc-RNA seq, we pooled FACS sorted Xcr1^{+} cDC1 cells from three organs of hyperlipidemic ApoE-deficient mice fed a HFD for 20 weeks, including the aorta, spleen, and lymph nodes, and Xcr1^{+} cDC1 cells from aorta and splenocytes of ApoE-deficient mice fed a chow diet. Libraries for sc-RNA seq were prepared using barcode oligos conjugated to anti-CD45 antibodies for surface staining so that samples from each type of organ could be compared in sequential analyses. Therefore, we had a total of five samples, and our focus was to understand the differences between Xcr1^{+} cDC1 cells from three different organs under hyperlipidemic conditions. The cells were sorted by gating Xcr1-positive cells out of the MHCII^{+}CD11c^{+} conventional dendritic cells (**Figure S8**). Firstly, we obtained the UMAP plot of 10 clusters of cDC1 cells using the Seurat 4.0 package (**Figure 5A**). In this analysis, 3830 quality-controlled

Xcr1$^+$ cDC1 cells were from three types of organs in hyperlipidemic mice, and an additional 2081 cells were from cDC1 cells sorted from the spleen and aorta of ApoE deficient mice fed on a chow diet. The clusters were differentiated according to top 10 differentially expressed genes (**Supplementary Table 2**), and the heatmap shows marker genes and heterogeneity among the 10 clusters of cDC1 cells (**Figure 5B**). The purpose of this experiment was to determine whether cDC1 cells from different organs possess unique features and whether cDC1 cells from aortic lesions can be characterized by the expression of marker genes. In hyperlipidemic mice, cDC1 cells from the spleen and lymph nodes differed quite dramatically in Cluster 2 (*Stk17b* and *Gpr171* highly expressing cells), where 28.9% of cDC1 cells from the spleen versus 1.0% of cDC1 cells from the lymph nodes were located. Conversely, 3.15% of cDC1 cells from the spleen versus 32.4% of cDC1 cells from the lymph nodes fell in Cluster 3 (*Ccl5* and *Epsti1* highly expressing cells), and 4.6% of cDC1 cells from the spleen versus 25.9% of cDC1 cells from the lymph nodes fell in Cluster 4 (*Slfn5* and *Ifi44* highly expressing cells). Despite the fact that we had only transcriptomic data for 68 Xcr1$^+$ cDC1 cells from aortic lesions, we were surprised to find that such aortic cDC1 mainly fell into Cluster 1, 4 and 5, comprising 80.8% of the cells analyzed (**Figure 5C**). In Cluster 1 (*Hspa1b* and *Dnajb1* highly expressing cells), where aortic cDC1 is dominantly enriched, the cDC1 cells sorted from lymph nodes were essentially absent, while in Cluster 4, aortic cDC1 cells were highly enriched and splenic cDC1 was obviously lower in percentage (**Figure 5C**). Cluster 7 (*Fabp5* and *S100a4* highly expressing cells) is exclusively comprised of cDC1 cells sourced from lymph nodes, with a striking absence of cDC1 cells from the spleen and aorta (**Figure 5C**). To better visualize the enrichment of aortic Xcr1$^+$ cDC1 cells distributed in a few clusters, we separately compared the three samples from the spleen, lymph

nodes, and aorta of hyperlipidemic mice using density plots. Interestingly, the Xcr1^{+} cDC1 cells from the spleen and lymph nodes displayed an obvious difference in their distribution, and aortic Xcr1^{+} cDC1 cells appeared more enriched in a few clusters (**Figure 5D-E**). Therefore, our data suggest that Xcr1^{+} cDC1 cells from the spleen and lymph nodes can differ markedly in heterogeneity, and aortic Xcr1^{+} cDC1 cells are enriched in a few clusters that express marker genes, *Ccr2*, *Sept3* and *Cldnd1* (**Supplementary Table 3**).

Together, these data implied that Xcr1^{+} cDC1 in the aorta originate from bone marrow, and Xcr1^{+} cDC1 cells exhibit strong heterogeneity among aorta, spleen and lymph nodes.

Knockout of Xcl1 attenuates the development of atherosclerosis in ApoE$^{-/-}$ mice

Xcl1 is the major chemokine involved in cDC1 recruitment [41, 42], and plays critical role in immune response with diverse physical and pathological implication through its interaction with the sole receptor, Xcr1 [43, 44]. We found the presence of Xcl1 in the lesion area in both human and mouse atherosclerotic lesions (data not shown). To elucidate the causal relationship between Xcl1 and Xcr1^{+} cDC1 in the development of atherosclerosis, and more importantly to experimentally verify Xcl1 as a potential therapeutic target for atherosclerosis treatment, we established the Xcl1 and ApoE double knockout mice. After being fed with a HFD for 19 weeks, both Xcl1$^{-/-}$ ApoE$^{-/-}$ and ApoE$^{-/-}$ mice were sacrificed to assess the severity of atherosclerosis. As shown in **Figure 6A-D**, the size of lesion at the descending aorta and aortic root was significantly smaller in Xcl1$^{-/-}$ ApoE$^{-/-}$ compared to that in ApoE$^{-/-}$ mice. Importantly, ORO staining of the liver, body weight and blood lipid profiles revealed no significant differences between the two groups (**Figure 6E-H**). Moreover, the IHC experiment result show the percentage of CD68 positive macrophages in aortic lesion was similar between two groups (**Figure 6I-J**).

Previous study identified that Xcl1 serves as a potent chemokine, selectively acting on cDC1 cells through its exclusive receptor, Xcr1 [42]. Consequently, we examined the DCs and the activation of T cells in different organs, including aorta, lymph node and spleen. The flow cytometric results illustrated that the frequencies of Xcr1^{+} cDC1 cells in the aorta were significantly reduced, but the frequencies of pDC and cDC2 cells from Xcl1$^{-/-}$ ApoE$^{-/-}$ were comparable with that from ApoE$^{-/-}$ (**Figure 7A-B**). Moreover, in both lymph node and spleen, the absolute numbers of pDC, cDC1 and cDC2 from Xcl1$^{-/-}$ ApoE$^{-/-}$ were comparable with that from ApoE$^{-/-}$ (**Figure S9**). The frequencies of CD8b^{+} T cells were also significantly lower, and CD4^{+} T cells were significantly higher, but the CD4^{+}CD69^{+} and CD8^{+} CD69^{+} T cells in the aorta from Xcl1$^{-/-}$ ApoE$^{-/-}$ mouse were comparable with that from ApoE$^{-/-}$ mouse (**Figure 7C-D**). Furthermore, the absolute numbers of CD4^{+}, CD8^{+}, CD4^{+} CD69^{+} and CD8^{+} CD69^{+} T cells in both lymph node and spleen from Xcl1$^{-/-}$ ApoE$^{-/-}$ mouse were comparable with that from ApoE$^{-/-}$ mouse (**Figure S10)**.

Collectively, these data suggested that Xcl1 could attenuate the development of atherosclerosis via reducing the recruitment of Xcr1^{+} cDC1 cells and CD8^{+} T cells in atherosclerotic lesions. More importantly, *in vivo* data demonstrated the promising potential of targeting Xcl1 to reduce the inflammatory response in atherosclerotic lesions. Our work paves the way to discover novel solutions for the treatment of atherosclerosis by targeting Xcl1 and Xcr1^{+} cDC1 cells.

Discussion

Atherosclerosis is a complex disorder, and understanding the role of the immune system, particularly dendritic cells (DCs), is of paramount importance [45, 46]. The marked diversity of DC subsets and their distinct, and at times contradictory functions pose challenges in clarifying the role of each specific type of DC in the context of atherosclerosis [47-53]. Moreover, the

restricted characterization of each subset of DCs in atherosclerosis, especially when compared to that in well-studied organs such as the skin and lymph nodes [13], has been severely hindered by the limited application of appropriate genetic models and *in vivo* data. Equally significant is that dissecting the functions of each subset of DCs *in vivo* relies on the development of genetic tools validated for lineage specificity. Recently, Xcr1$^+$ cDC1 has been extensively investigated using the Cre line under the promoter of the Xcr1, despite well-documented expression leakiness [20, 31]. Compelling evidence from tumor and viral infection models [14, 41, 54-56], as well as metabolic disorders like non-alcoholic steatohepatitis [57], has demonstrated the critical role of Xcr1$^+$ cDC1 cells in diseases. Nevertheless, the precise role of Xcr1$^+$ cDC1 cells in atherosclerosis remains undetermined.

The precise characterization of Xcr1$^+$ cDC1 and its functions within the atherosclerotic milieu could provide valuable insights into the immunopathogenesis of the disease. By delineating the specific contributions of Xcr1$^+$ cDC1, we may identify novel therapeutic targets and develop more targeted and effective strategies for the prevention and treatment of atherosclerosis. Therefore, investigation to understand the roles of Xcr1$^+$ cDC1 in the context of atherosclerosis and to identify therapeutic targets is highly warranted. However, at least two major obstacles impede the *in vivo* study of Xcr1$^+$ cDC1 in atherosclerotic mice. First, Xcr1$^+$ cDC1 cells are extremely scarce in number, and it is quite challenging to obtain highly purified Xcr1$^+$ cDC1 cells from aortic plaque in hyperlipidemic mice. Second, there are very few appropriate genetic model systems that permit functional analyses of Xcr1$^+$ cDC1 *in vivo*. Earlier studies on the role of Xcr1$^+$ cDC1 cells in atherosclerosis have yielded conflicting results, largely due to the use of different mouse models. For instance, the deletion of Batf3, Irf8, Dngr1, or Flt3 decreased the cDC1 cells. Nevertheless,

Batf3 deficiency had no impact on atherosclerosis in hyperlipidemic mice. In contrast, Irf8 or Dngr1 deficiency reduced the development of atherosclerosis, while Flt3 deficiency exacerbated the condition [15-19]. The recently developed Xcr1-Cre was found to have leakiness of recombinase activity in other immune cells [20]. Here, we optimized the design for the construction of the Cre line using the endogenous promoter of Xcr1 and validated its fidelity under hyperlipidemic conditions. We crossed the novel knock-in line termed $Xcr1^{Cre\text{-}Gfp}$ with $Rosa26^{LSL\text{-}tdRFP}$ Cre reporter mice and used the resulting F1 hybrids as bone marrow donors. The bone marrow cells were then transferred into $ApoE^{-/-}$ mice, which were subsequently fed on a HFD. We monitored the Cre recombinase activity, which was reflected by the tdRFP expression of this novel mouse line. Under hyperlipidemic conditions, we did not observe any leakiness of Cre activity, as tdRFP was strictly restricted to cDC1 cells. To the best of our knowledge, this novel Cre line is the first of its kind. We further crossed the $Xcr1^{Cre\text{-}Gfp}$ and $Rosa26^{LSL\text{-}DTA}$ mice with $ApoE^{-/-}$ mice respectively. Subsequently, by further crossing, we obtained $Xcr1^{Cre\text{-}Gfp}$ $Rosa26^{LSL\text{-}DTA}$ $ApoE^{-/-}$ mice to create a complex genetic model, in which $Xcr1^{+}$ cDC1 is depleted *in vivo* in the context of atherosclerosis. Very interestingly, in the $Xcr1^{+}$ cDC1 depleted mice, atherosclerosis was significantly ameliorated. Coupled with the data we obtained from murine and human samples, where $Xcr1^{+}$ cDC1 cells exist in the aortic plaque and their accumulation is correlated with disease progression, we conclude that $Xcr1^{+}$ cDC1 is essential for the development of atherosclerosis.

Despite the fact that $Xcr1^{+}$ cDC1 cells are extremely rare in number, we were inclined to understand if there were any differences among $Xcr1^{+}$ cDC1 cells from different organs. We compared, under hyperlipidemic conditions, the $Xcr1^{+}$ cDC1 cells sorted from the spleen and

lymph nodes, supplemented by a small number of but well-purified Xcr1$^+$ cDC1 cells from aortic lesions. To our surprise, the clusters of Xcr1$^+$ cDC1 displayed obvious distinctions among different organs. When the Xcr1$^+$ cDC1 cells from aortic lesions were projected to the clusters, we found that the major subsets present in the lymph nodes, characterized by the expression of markers *Ccl5 and Fabp5*, and in the spleen, marked by *Stk17b* and *Gpr171*, were basically absent in the aorta. Meanwhile, compared with spleen and lymph nodes, the aortic Xcr1$^+$ cDC1 cells are highly expressed Ccr2, which is an extremely important chemokine receptor dominating monocyte homing [58-60]. Using the bone marrow transfer model, we also determined that the Xcr1$^+$ cDC1 in the aortic plaque is replenished by circulating precursors.

In other disease models, Xcr1$^+$ cDC1 cells are crucial for activating T cells [55, 61], and we confirmed that in hyperlipidemic mice, the depletion of cDC1 led to a significant inhibition of T cell activation. It is important to note that Xcr1$^+$ cDC1 cells are known for well-established role in cross-presentation to CD8$^+$ T cells, recent studies have shown Xcr1$^+$ cDC1 cells also engage with CD4$^+$ T cells [20, 27]. Our data showing Xcr1$^+$ cDC1-dependent CD4 and CD8 T cell activation in atherosclerotic plaques is in line with the new paradigm for cDC1s as a platform for both CD4 and CD8 T cell responses in the novel context of atherosclerosis. Considering the multifaceted roles of macrophages in lipid metabolism, inflammation, and plaque dynamics during the development of atherosclerosis [62], we evaluated the presence of macrophages in atherosclerotic lesions using IHC and flow cytometry. Our results indicated comparable proportions of macrophages in the aorta between Xcr1$^+$ cDC1 depleted mice and ApoE$^{-/-}$ control mice. Additionally, our results also demonstrated that the loss of Xcr1$^+$ cDC1 cells did not affect lipid status.

Since we elucidated the critical role of Xcr1^{+} cDC1 cells in atherosclerosis, our aim was to test the therapeutic potential of inhibiting this specific cell type during disease progression. As Xcr1 is the sole receptor for Xcl1, and Xcl1 selectively attracts Xcr1^{+} cDC1 cells in both mice and humans [44, 63], we performed Xcl1 knockout on the background of ApoE deficient mice and assessed the impact on atherosclerosis development. We found that the Xcl1-Xcr1 axis plays a crucial role in the progression of atherosclerosis. Our results demonstrated that the loss of Xcl1 in hyperlipidemic ApoE$^{-/-}$ mice significantly reduced atherosclerotic lesion formation, decreased the frequencies of Xcr1^{+} cDC1 cells and CD8^{+} T cells in the aorta, without affecting lipid status or the number of aortic macrophages. Our findings indicate that Xcl1 could potentially serve as an effective target for the treatment of atherosclerosis.

Materials and Methods

Animal experiments and patients

All mice were raised in a Specific Pathogen-Free facility and the experiments were conducted in accordance with the guidelines approved by the Animal Ethics Committee of Xinxiang Medical University (China) (Reference No. XYLL-2016S001). The sections of the human femoral artery were obtained in accordance with our previous study [30] and approved by the Ethics Committee of the Third Military Medical University (Project identification code SYXK-PLA-20170005). Rosa26$^{LSL\text{-}RFP}$ knock-in mice were generously provided by Hervé Luche at University Clinics Ulm in Germany [32]. C57BL/6 and ApoE$^{-/-}$ mice were purchased from Beijing Vital River Laboratory Animal Technology (China). Rosa26$^{LSL\text{-}DTA}$ knock-in mice (Stock Number 009669) were purchased from the Jackson Laboratory (United States of America). Both HFD (contained 20%

protein, 20% carbohydrate, 40% fat and 1.25% cholesterol, Cat: XT108C), and chow diet (contained 20% protein, 64% carbohydrate, 20% fat, Cat: AIN-93G) were purchased from Jiangsu Xietong Pharmaceutical Bioengineering Co., Ltd. 7-8 weeks old mice were used to establish atherosclerosis model through fed on a HFD for 8-20 weeks. On harvest, each sample was assigned an analytical code that was irrelevant to its genotype and processed and analyzed by a researcher blinded to its origin.

Generation of Xcr1$^{Cre\text{-}Gfp}$ knock-in mice

The Xcr1$^{Cre\text{-}Gfp}$ mouse line was generated by inserting a Cre-P2A-GFP-P2A cassette immediately upstream of the endogenous *Xcr1* translational start codon (ATG). This design enables co-expression of Cre recombinase and GFP under the control of the native *Xcr1* promoter. A 3.2-kb repair template was synthesized (GenScript, Nanjing, China), consisting of a 0.62-kb 5' homology arm (HA), a codon-optimized *Cre* sequence fused to a P2A peptide, an enhanced GFP reporter linked to a second P2A site, and a 0.67-kb 3' homology arm. For targeted integration, CRISPR/Cas9-mediated homology-directed repair (HDR) was performed by co-injecting Cas9 mRNA, a chimeric sgRNA (sgXcr1-KI), and the repair template into fertilized C57BL/6 zygotes at the one-cell stage, following established protocols[64, 65]. Founders (F0) harboring the correct knock-in allele were identified by PCR and Sanger sequencing, then used to establish heterozygous lines. The sgRNA sequence is provided in **Supplementary Table 1**.

Breeding strategy of Xcr1$^{Cre\text{-}Gfp}$ Rosa26$^{LSL\text{-}DTA}$ ApoE$^{-/-}$

To generate Xcr1$^{Cre\text{-}Gfp}$ Rosa26$^{LSL\text{-}DTA}$ ApoE$^{-/-}$ mice, we performed the following crosses: Xcr1$^{Cre\text{-}Gfp}$ mice were crossed with ApoE$^{-/-}$ mice, and offspring heterozygous for both alleles were

intercrossed to obtain homozygous Xcr1$^{Cre\text{-}Gfp}$ ApoE$^{-/-}$ mice. Rosa26$^{LSL\text{-}DTA}$ mice were crossed with ApoE$^{-/-}$ mice, and progeny heterozygous for both alleles were intercrossed to generate homozygous Rosa26$^{LSL\text{-}DTA}$ ApoE$^{-/-}$ mice. Finally, homozygous Xcr1$^{Cre\text{-}Gfp}$ ApoE$^{-/-}$ mice were crossed with homozygous Rosa26$^{LSL\text{-}DTA}$ ApoE$^{-/-}$ mice to produce Xcr1$^{Cre\text{-}Gfp}$ Rosa26$^{LSL\text{-}DTA}$ ApoE$^{-/-}$ offspring.

Generation of Xcl1 knockout mice

The Xcl1 knockout mouse line was generated using CRISPR/Cas9 genome editing through the microinjection of a mixture containing Cas9 mRNA and two sgRNAs into fertilized C57BL/6 zygotes at the one-cell stage, as previously described [66]. The genotypes were confirmed using PCR and Sanger sequencing. Subsequently, Xcl1 and ApoE double knockout mice were obtained by crossing the Xcl1$^{-/-}$ mice with ApoE$^{-/-}$ mice. The sequences of the sgRNA are reported in **Supplementary Table 1**.

Bone marrow transplantation

After one week of antibiotic treatment, the recipient CD45.1^{+} CD45.2^{+} ApoE$^{-/-}$ mice were injected intraperitoneally with busulfan at a dosage of 30 μg/g every two days for one week. Subsequently, bone marrow from 8-week-old CD45.2^{+} Xcr1$^{Cre\text{-}Gfp}$ Rosa26$^{LSL\text{-}RFP}$, CD45.2^{+} Xcr1$^{Cre\text{-}Gfp}$ Rosa26$^{LSL\text{-}DTA}$ or WT (CD45.2^{+} wild-type) donor mice was intravenously transferred to each recipient mouse, with two million cells administered per recipient. The efficiency of transplantation was assessed four-week post-transplantation, after which all mice were fed a HFD for 16 weeks. Finally, the mice were sacrificed for *en face* analysis of the descending aorta, hematoxylin and eosin (H&E) staining, Oil Red O (ORO) staining of the aortic root, and flow

cytometry analysis, as previously described [67].

Immunofluorescence

Frozen sections of the aortic root from mice were incubated at 60 °C for 2 minutes and then fixed in 4% paraformaldehyde for 30 minutes. The samples were subsequently washed with PBS and permeabilized/blocked with 0.1% Triton X-100 in 5% BSA. Next, the primary antibodies, including anti-Xcr1 (BD Biosciences, Cat. 148212) and anti-CD11c (BD Biosciences, Cat. 12-0114-83), were applied in a wet box at 4 °C overnight. After washing with PBST (PBS containing 0.1% Tween-20) for five times, the samples were incubated with secondary antibodies for 1 hour, followed by a 10-minute incubation with DAPI at room temperature (protected from light). The fluorescent signals of the sections were detected using a Nikon C2 confocal microscope (Nikon, Japan).

Morphometric and immunohistochemical analyses

After modeling, the heart and aorta tissue were obtained from mice. The *en face* descending aortas were fixed with 4% paraformaldehyde and subsequently stained with ORO. Additionally, frozen sections of the aortic roots were stained with ORO and H&E to assess the severity of atherosclerosis, and frozen sections of livers were stained with ORO to assess the severity of lipid accumulation, in accordance with our previous study [67]. Paraffin-embedded sections of the aortic root were dewaxed in xylene twice for 10 minutes, rehydrated through descending grades of ethanol, and subjected to sodium citrate-induced antigen retrieval for 10 minutes at 95 °C. The sections were then incubated with 3% H_2O_2 for 10 minutes at room temperature. Following this, the sections were blocked and incubated with primary antibodies, either anti-Xcr1 (NBP1-02343)

or CD68 (FB113109). After five washes with DPBS, the sections were incubated with secondary antibodies for 30 minutes and stained with DAB at room temperature. Subsequently, the sections were counterstained with hematoxylin, dehydrated in ethanol, and mounted with neutral balsam. Images were captured using the digital pathology system (Pannoramic MIDI, Hungary), viewed using CaseViewer2.4 software and analyzed using ImageJ software.

Flow cytometry analysis

To obtain the single-cell suspension, aortas, lymph nodes and spleens were collected from each mouse. Spleens were directly dissociated using the Gentle MACS Dissociators (Miltenyi Biotec). Aortas and lymph nodes were cut into small pieces and then dissociated using the Gentle MACS Dissociators. Dissociated tissues digested with digestive enzymes (Collagenase IV, Cat: V900893 from Sigma; DNase I, Cat: DN25 from Sigma; Liberase DH, Cat: 5401054001 from Roche) for 30 minutes at 37 °C using a shaker set to 300 rpm or a heating block. The resulting cell suspension was filtered through 75 μm strainers and subsequently blocked with 2.4G2 for 20 minutes at 4 °C, followed by washing with stain buffer (BD, Cat: 554656). Then samples were stained with monoclonal antibody mixes for 30 minutes at 4 °C followed by washing with stain buffer. Finally, cells were resuspended in stain buffer containing 200 nM Sytox blue (ThermoFisher Scientific, Cat: S34857) and acquired using a flow cytometer (ThermoFisher Scientific, Invitrogen Attune NxT Flow Cytometer), and the FACS data were analyzed using FlowJo software. The following antibodies purchased from BioLegend, BD or eBioscience were used to detect surface markers by flow cytometry: anti-CD45.2 (104) conjugated to eFluor 450, FITC or PE-Cy7; anti-CD45.1 (A20) conjugated to PE or eFluor450; anti-CD45 (30-F11) conjugated to PE; anti-CD11b (M1/70) conjugated to super Bright 600, BUV395 or biotin; anti-CD3e (145-2C11) conjugated to

PE-Cy5.5 or PE-Cy7; anti-CD3e (eBio500A2) conjugated to Alexa Fluor700; anti-CD19 (eBio1D3) conjugated to PE-Cy5.5 or biotin; anti-Xcr1 (ZET) conjugated to APC or BV650; anti-Ly6G (1A8) conjugated to Alexa Fluor 700; anti-MHCII (M5/114.15.2) conjugated to APC-eFluor780; anti-CD11c (N418) conjugated to PE or PE-Cy5.5; anti-Siglec H (eBio440c) conjugated to PE-Cy7 or PE; anti-CD8b (eBioH35-17.2) conjugated to eFluor 450; anti-CD44 (IM7) conjugated to BV605; anti-CD4 (RM4-5) conjugated to PE-Cy5.5; anti-CD69 (H1.2F3) conjugated to PE-Cy7; anti-CD62L (MEL-14) conjugated to APC; anti-CD5 (53-7.3) conjugated to APC-eFluor780 or biotin; anti-Siglec F (E50-2440) conjugated to BV421; anti-F4/80 (BM8) conjugated to PE-Cy7; anti-CD64 (X54-5/7.1) conjugated to APC; anti-NK1.1 (PK136) conjugated to Alexa Fluor 700; anti-CD172α (P84) conjugated to FITC.

Single cell RNA sequencing

Eight-week-old male ApoE$^{-/-}$ mice were fed with 20-week chow diet or HFD. The single cell suspension of spleen, lymph node and aorta were obtained according to the flow cytometry analysis section. Single cell suspension from spleens and lymph nodes were firstly removed the CD5^{+}, CD19^{+} and CD11b^{+} cells via SAV conjugated beads. Then two million live cells from spleen and lymph node were stained with mix1 (CD45.2-PE-Cy7, CD11c-PE-Cy5.5, CD172α-FITC, MHCII- APC-eFluor780 and Xcr1-APC), and all cells from aorta were stained with mix2 (CD45.2-PE-Cy7, CD11b-super bright 600, CD11c-PE-Cy5.5, MHCII- FITC, CD3-Alexa Fluor 700, CD19- Alexa Fluor 700, Ly6G- Alexa Fluor 700 and Xcr1-APC) for 30 minutes at 4 °C. After washing with 1 mL FACS buffer two times, cells from different organs were stained with different anti-CD45 antibodies conjugated with barcode oligos from BD™ Ms Single Cell Sample Multiplexing Kit (BD Bioscience, Cat: 633793). Finally, cells were resuspended with

Sytox blue and $CD11c^+$ $MHCII^+$ $Xcr1^+$ cells were sorted and subjected to the BD Rhapsody Express system. Then cDNA and sample tag libraries were built with BD Rhapsody whole transcriptome amplification (WTA) reagent kit (BD Bioscience, Cat: 633733, 633773, 633801, 664887) following manufacturer's instructions, and sequenced on an illumine Novaseq 600 sequencer. Pair-end Fastq files of sample tag and WTA data were processed via BD Rhapsody™ analysis pipeline v2.0, and the resultant dataset was mainly analysis using SeqGeq™ software, which contain Lex-BDSMK and Seurat v4.04 plugin components. Raw data and processed data were uploaded into GEO (Accession number: GSE279370).

Statistical analysis

All data were presented as means ± SEM (Standard Error of the Mean), reflecting the average values of biological measurements across multiple samples. Data analysis was performed using GraphPad Prism software (version 8.0). Statistical significance was assessed by both parametric (unpaired Student's *t*-test) and nonparametric (Mann–Whitney test) methods when comparing two groups. The assumptions of the tests were checked to ensure appropriate application. Significant differences between different groups were set at * $P<0.05$, ** $P<0.01$, *** $P<0.001$ and **** $P<0.0001$. Graphical representations of the data will include bar graphs with error bars denoting SEM.

Acknowledgements

We thank the animal facility and flow cytometry facility of GRIS in Xinxiang Medical University for providing technical support and assistance. Generation of murine genetic models were supported by 111 program (D20036).

Author Contributions

Lichen Zhang and **Yinming Liang** conceived the project. **Tianhan Li** and **Liaoxun Lu** wrote the manuscript and carried out the majority of the experiments. **Bernard Malissen** and **Lichen Zhang** designed the Xcr1Cre-Gfp knock-in mice and Xcl1 knockout mice. **Juanjuan Qiu**, **Xin Dong**, **Le Yang**, **Kexin He**, and **Yanrong Gu** assisted in the experimental procedures. **Binhui Zhou** performed cell sorting for scRNA sequencing. **Tingting Jia** and **Rong Huang** contributed to data curation and validation. **Toby Lawrence**, **Marie Malissen**, and **Hui Wang** participated in the manuscript review and editing. **Guixue Wang** assisted in the preparation of human samples. **Yinming Liang**, **Lichen Zhang**, and **Tianhan Li** contributed to obtaining the funding for the project.

Sources of Funding

This research was funded by projects 2022WZ1021 and 2023DK2005 to YL, 2022RC1223 to LZ, 242102310030 to TL, and the NSFC grants 82301972 and 32170879 to TL and LZ.

Declaration of competing interest

The authors declare no competing interests.

Figure legends

Figure 1. Progressive accumulation of Xcr1^{+} cDC1 cells in human and mouse advanced atherosclerotic lesions

A, Representative images of immunohistochemical staining demonstrate Xcr1 expression in normal areas and plaque areas of the femoral artery from three cardiovascular disease patients. **B**, Quantitative analysis of the Xcr1-positive area in normal area and plaque regions. **C**, Representative immunofluorescence images depict DAPI (blue), Xcr1 (green) and CD11c (red) within the lesions of aortic root of ApoE$^{-/-}$ mice fed with 16-week chow diet or HFD. **D**, Quantitative analysis of Xcr1 and CD11c double positive area in lesion area (n = 6). Scale bars, 100 μm. **E**, Representative images depicting immunohistochemical staining of Xcr1 in lesions of the aortic root of ApoE$^{-/-}$ mice fed a HFD for varying durations. **F**, Quantitative analysis of the Xcr1-positive area in the lesion regions. (HFD-8W mice, n = 11; HFD-12W mice, n = 15; HFD-16W mice, n = 29). Data represent as mean ± SEM. *** P<0.001.

Figure 2. Selective expression of Xcr1$^{Cre\text{-}Gfp}$ in cDC1 cells.

A, Diagram illustrating the bone marrow transfer process. **B** and **C**, Representative flow cytometric analysis and corresponding quantification of GFP^{+}RFP^{+} in cDC1 and non-cDC1 populations within the cDC1 and non-cDC1 populations of the spleen. These data were obtained from ApoE$^{-/-}$ mice that had received bone marrow transplants from either WT or Xcr1$^{Cre\text{-}Gfp}$ Rosa26$^{LSL\text{-}RFP}$ donors and were maintained on a HFD for 16 weeks (WT, n = 4; Xcr1$^{Cre\text{-}Gfp}$ Rosa26$^{LSL\text{-}RFP}$, n = 3). **D** through **F**, Eight-week-old ApoE$^{-/-}$, Xcr1$^{Cre\text{-}Gfp}$ ApoE$^{-/-}$ and Xcr1$^{Cre\text{-}Gfp}$ Rosa26$^{LSL\text{-}DTA}$ ApoE$^{-/-}$ mice fed with a HFD for 16 weeks (n = 3). **D** and **E**, Representative flow

cytometric analysis and quantification of the percentage of GFP^+ cells among pDC, cDC1 and cDC2 cells populations in the spleen. **F**, Quantification of the percentage of pDC, cDC1 and cDC2 cells in spleen. Data represent as mean ± SEM. **** *P*<0.0001; NS, non-significant.

Figure 3. Specific depletion of $Xcr1^+$ cDC1 cells in $ApoE^{-/-}$ mice reduces atherosclerosis progression with no effect on macrophages.

A through **I**, Eight-week-old $ApoE^{-/-}$ mice and $Xcr1^{Cre\text{-}Gfp}$ $Rosa26^{LSL\text{-}DTA}$ $ApoE^{-/-}$ mice were fed on a 16-week HFD to develop atherosclerosis. **A**, ORO staining of the descending aortas. Scale bar, 5 mm. **B**, Quantification of the lesion area in the descending aorta ($ApoE^{-/-}$ mice, n = 9; $Xcr1^{Cre\text{-}Gfp}$ $Rosa26^{LSL\text{-}DTA}$ $ApoE^{-/-}$ mice, n = 6). **C**, ORO and H&E staining of the aortic roots of representative mice from each group. **D**, Quantification of lesion area in the aortic root. ($ApoE^{-/-}$ mice, n = 7; $Xcr1^{Cre\text{-}Gfp}$ $Rosa26^{LSL\text{-}DTA}$ $ApoE^{-/-}$ mice, n = 8). Scale bar, 200 μm. **E** and **F**, H&E staining and quantification of necrotic core area in the lesions of aortic root. ($ApoE^{-/-}$ mice, n = 7; $Xcr1^{Cre\text{-}Gfp}$ $Rosa26^{LSL\text{-}DTA}$ $ApoE^{-/-}$ mice, n = 8). Scale bar, 200 μm. **G** and **H**, Representative flow cytometric analysis and quantification of macrophages in the aorta. ($ApoE^{-/-}$ mice, n = 8; $Xcr1^{Cre\text{-}Gfp}$ $Rosa26^{LSL\text{-}DTA}$ $ApoE^{-/-}$ mice, n = 6). **I** and **J,** Representative immunohistochemical staining images of CD68 and quantification of CD68 positive area in the lesions of the aortic root. ($ApoE^{-/-}$ mice, n = 6; $Xcr1^{Cre\text{-}Gfp}$ $Rosa26^{LSL\text{-}DTA}$ $ApoE^{-/-}$ mice, n = 8). Scale bar, 100 μm. Data represent as mean ± SEM. NS, non-significant.

Figure 4. Specific depletion of $Xcr1^+$ cDC1 cells in $ApoE^{-/-}$ mice decreases T cell activation within aorta.

A through **D**, Eight-week-old ApoE$^{-/-}$ mice and Xcr1$^{Cre\text{-}Gfp}$ Rosa26$^{LSL\text{-}DTA}$ ApoE$^{-/-}$ mice fed a HFD for 16 weeks. **A**, Representative flow cytometric analysis cDC1 cells in aortas. **B**, Quantification of cDC1 cells in aorta (n = 4). **C**, Representative flow cytometric analysis T cells in aortas **D**, Quantification of T cell populations, including CD4^{+}, CD4^{+}CD69L^{+}, CD8b^{+} and CD8b^{+}CD69L^{+} T cells in aortas (n = 7). Data represent as mean ± SEM. * P<0.05, ** P<0.01, *** P<0.001, ns, non-significant.

Figure 5. Sc-RNA sequencing analysis of the aorta, lymph nodes and spleen in ApoE$^{-/-}$ mice fed with a 20-week HFD.

A, UMAP plot delineates 10 annotated cell types of CD11c^{+} MHCII^{+} Xcr1^{+} cDC1 cells from aorta, lymph node and spleen in ApoE$^{-/-}$ mice maintained on a HFD for 20 weeks. **B**, Heatmap statistic map displays the top ten up-regulated genes across various clusters. **C**, Histogram plot illustrates the proportion of different cell types among groups. **D** and **E**, UMAP plot representing CD11c^{+} MHCII^{+} Xcr1^{+} cDC1 cells from aorta, lymph nodes, spleen, and a merged plot in ApoE$^{-/-}$ mice maintained on a HFD for 20 weeks.

Figure 6. Xcl1 deficiency reduces atherosclerotic lesion formation in ApoE$^{-/-}$ mice.

A through **I**, Eight-week-old ApoE$^{-/-}$ mice and Xcl1$^{-/-}$ ApoE$^{-/-}$ mice fed a HFD for 19 weeks (n = 8 per group). **A**, ORO staining of the descending aortas. Scale bar, 5 mm. **B**, Quantification of the lesion area in aortas. **C**, ORO and H&E staining of aortic roots. Scale bar, 200 μm. **D**, Quantification of the lesion area in aortic roots. **E** and **F**, Representative liver images and quantification of ORO positive area in livers (n = 24 regions from 8 mice, 3 regions per mice).

Scale bar, 100 μm. **G**, The concentrations of TC, TG, LDL and HDL in the serum. **H**, Body weight of mice before and after feeding with 19-week HFD. **I**, Representative immunohistochemical staining of CD68 in aortic roots. **J**, Quantification of CD68 positive area in the lesions of aortic roots (n = 24 lesions from 8 mice, 3 lesions per mice). Scale bar, 100 μm. Data represent as mean ± SEM. ** $P<0.01$, *** $P<0.001$, NS, non-significant.

Figure 7. Xcl1 deficiency reduces CD8$^+$ T cells frequency in the aorta from.

A through **D**, Eight-week-old ApoE$^{-/-}$ mice and Xcl1$^{-/-}$ApoE$^{-/-}$ mice fed with a 16-week HFD. (n = 7). **A** and **B**, Representative flow cytometric analysis and quantification of pDC, cDC1 and cDC2 cells in aortas. **C** and **D**, Representative flow cytometric analysis and quantification of T cell subsets, including CD4$^+$, CD4$^+$ CD69L$^+$, CD8b$^+$ and CD8b$^+$ CD69L$^+$ T cells in aortas. Data represent as mean ± SEM. * $P<0.05$, NS, non-significant.

Figure S1. Schematic diagram illustrating the knock-in of the 5'HA-iCre-P2A-EGFP-P2A-3'HA vector into the mouse Xcr1 locus.

Figure S2. Flow cytometric analysis of cDC1 cells in the lymph nodes and spleens of ApoE$^{-/-}$ mice and Xcr1$^{Cre\text{-}Gfp}$ Rosa26$^{LSL\text{-}DTA}$ ApoE$^{-/-}$ mice fed a 7-weeks chow diet.

A through **D**, ApoE$^{-/-}$ mice and Xcr1$^{Cre\text{-}Gfp}$ Rosa26$^{LSL\text{-}DTA}$ ApoE$^{-/-}$ mice fed with a 7-week chow diet. (n = 7). **A**, Representative flow cytometric analysis of cDC1 cells in lymph nodes. **B**, Quantification of the frequencies and number of cDC1 cell in lymph nodes. **C**, Representative flow cytometric analysis cDC1 cells in the spleens. **D**, Quantification of the frequencies and

number of cDC1 cell in the spleens. Data represent the mean ± SEM. *** *P*<0.001.

Figure S3. Lipid profile, body weight and ORO staining of the liver in ApoE$^{-/-}$ mice and Xcr1$^{Cre\text{-}Gfp}$ Rosa26$^{LSL\text{-}DTA}$ ApoE$^{-/-}$ mice fed a 16-week HFD.

A through **D**, Eight-week-old ApoE$^{-/-}$ mice (n =7) and Xcr1$^{Cre\text{-}Gfp}$ Rosa26$^{LSL\text{-}DTA}$ ApoE$^{-/-}$ mice (n =8) were fed on a 16-week HFD to develop atherosclerosis. **A**, Concentrations of TC, TG, LDL and HDL in the serum. **B**, Body weight measurements of both groups of mice. **C**, ORO staining of liver from each group. Scale bar, 100 μm. **D**, Quantification of ORO positive area in liver. Data represent the mean ± SEM. ** *P*<0.01, *** *P*<0.001, NS, non-significant.

Figure S4. Flow cytometric analysis of cDC1 cells in the lymph nodes and spleens of ApoE$^{-/-}$ and Xcr1$^{Cre\text{-}Gfp}$ Rosa26$^{LSL\text{-}DTA}$ ApoE$^{-/-}$ mice fed a 16-week HFD.

A through **D**, Eight-week-old ApoE$^{-/-}$ mice (n =7) and Xcr1$^{Cre\text{-}Gfp}$ Rosa26$^{LSL\text{-}DTA}$ ApoE$^{-/-}$ mice (n =8) were fed on a 16-week HFD to develop atherosclerosis. **A**, Representative flow cytometric analysis of cDC1 cells in lymph nodes. **B**, Quantification of the frequencies and numbers of cDC1 cells in lymph nodes. **C**, Representative flow cytometric analysis of cDC1 cells in the spleens. **D**, Quantification of the frequencies and numbers of cDC1 cells in the spleens. Data represent the mean ± SEM. ** *P*<0.01, *** *P*<0.001, NS, non-significant.

Figure S5. Flow cytometric analysis of T cells in the lymph nodes and spleens of ApoE$^{-/-}$ mice and Xcr1$^{Cre\text{-}Gfp}$ Rosa26$^{LSL\text{-}DTA}$ ApoE$^{-/-}$ mice fed a 16-week HFD.

A through **F**, Eight-week-old ApoE$^{-/-}$ mice (n =7) and Xcr1$^{Cre\text{-}Gfp}$ Rosa26$^{LSL\text{-}DTA}$ ApoE$^{-/-}$ mice (n

=8) were fed on a 16-week HFD to develop atherosclerosis. **A**, Representative flow cytometric analysis of $CD4^+$, $CD8^+$, $CD4^+CD69^+$ and $CD8^+CD69^+$ T cells in lymph nodes. **B** and **C**, Quantification of the frequencies and numbers of $CD4^+$, $CD8^+$, $CD4^+$ $CD69^+$ and $CD8^+$ $CD69^+$ T cells in lymph nodes. **D**, Representative flow cytometric analysis and quantification of $CD4^+$, $CD8^+$, $CD4^+$ $CD69^+$ and $CD8^+$ $CD69^+$ T cells in the spleens. **E** and **F**, Quantification of the frequencies and numbers of $CD4^+$, $CD8^+$, $CD4^+$ $CD69^+$ and $CD8^+CD69^+$ T cells in the spleens. Data represent the mean ± SEM. * $P<0.05$, ** $P<0.01$, *** $P<0.001$, NS, non-significant.

Figure S6. T cells analysis in the lymph nodes and spleens of $ApoE^{-/-}$ mice and $Xcr1^{Cre\text{-}Gfp}$ $Rosa26^{LSL\text{-}DTA}$ $ApoE^{-/-}$ mice fed a 7-week chow diet.

A through **F**, $ApoE^{-/-}$ mice and $Xcr1^{Cre\text{-}Gfp}$ $Rosa26^{LSL\text{-}DTA}$ $ApoE^{-/-}$ mice fed with a 7-week chow diet. (n = 7). **A**, Representative flow cytometric analysis and quantification of $CD4^+$, $CD4^+$ $CD44^+$ $CD62L^-$, $CD8^+$ and $CD8^+$ $CD44^+$ $CD62L^-$ T cells in lymph nodes. **B**, Quantification of the frequencies of $CD4^+$, $CD8^+$, $CD4^+CD69^+$ and $CD8^+CD69^+$ T cells in the lymph nodes. **C**, Representative flow cytometric analysis and quantification of $CD4^+$, $CD4^+$ $CD44^+$ $CD62L^-$, $CD8^+$ and $CD8^+$ $CD44^+$ $CD62L^-$ T cells in the spleens. **D**, Quantification of the frequencies of $CD4^+$, $CD8^+$, $CD4^+$ $CD69^+$ and $CD8^+$ $CD69^+$ T cells in the spleens. **E** and **F**, Quantification of the numbers of $CD4^+$ and $CD8^+$ T cells in the lymph nodes and spleens. Data represent the mean ± SEM. * $P<0.05$, ** $P<0.01$, NS, non-significant.

Figure S7. Depletion of Xcr1^{+} cDC1 cells of bone marrow reduces cDC1 cells without affecting macrophages in atherosclerotic lesion of ApoE$^{-/-}$ mice.

A, Diagram of the bone marrow transfer process. ApoE$^{-/-}$ mice transplanted with bone marrow from WT or Xcr1$^{Cre\text{-}Gfp}$ Rosa26$^{LSL\text{-}DTA}$ donors before and after 16 weeks on a HFD (n = 7). **B**, Body weight of each group. **C**, Serum concentrations of TC, TG, LDL and HDL. **D**, Representative ORO staining images of liver sections and quantification of the ORO positive area percentage in the liver. Scale bar, 50 μm. **E**, Representative flow cytometric analysis of pDC, cDC1 and cDC2 cells in the aortas, Lin^{-} means CD3^{-} CD19^{-} Ly6G^{-} NK1.1^{-}. **F**, Representative flow cytometric analysis of macrophages in the aortas of each group. Data represent as mean ± SEM. *** P<0.001, NS, non-significant.

Figure S8. The single-cell RNA sequencing process.

Figure S9. DC cells analysis in lymph nodes and spleens of ApoE$^{-/-}$ and Xcl1$^{-/-}$ ApoE$^{-/-}$ mice fed with 19-week HFD.

A through **D**, Eight-week-old ApoE$^{-/-}$ (n = 9) and Xcl1$^{-/-}$ ApoE$^{-/-}$ mice (n = 7) fed a HFD for 19 weeks. **A**, Representative flow cytometric analysis and quantification of pDC, cDCs, cDC1 and cDC2 cells in lymph nodes. **B**, Quantification of absolute counts of pDC, cDCs, cDC1 and cDC2 cells in lymph nodes. **C**, Representative flow cytometric analysis of pDC, cDC1 and cDC2 cells in spleens. **D**, Quantification of absolute counts of pDC, cDCs, cDC1 and cDC2 cells in spleens. Data represent the mean ± SEM. NS, non-significant.

Figure S10. T cells analysis in lymph node and spleen of ApoE$^{-/-}$ and Xcl1$^{-/-}$ ApoE$^{-/-}$ mice fed with 16-week HFD.

A through **D**, Eight-week-old ApoE$^{-/-}$ (n = 9) and Xcl1$^{-/-}$ ApoE$^{-/-}$ mice (n = 7) fed a HFD for 19 weeks. **A** and **B**, Representative flow cytometric analysis and quantification of absolute counts of CD4^{+}, CD8^{+}, CD4^{+}CD69^{+} and CD8^{+}CD69^{+} T cells in lymph nodes. **C** and **D**, Representative flow cytometric analysis and quantification of absolute counts of CD4^{+}, CD8^{+}, CD4^{+}CD69^{+} and CD8^{+}CD69^{+} T cells in spleens. Data represent the mean ± SEM. NS, non-significant.

Supplementary table 1: **The sequences of the sgRNA and primers used for generation and validation of Xcr1$^{Cre\text{-}Gfp}$ knock-in mice and Xcl1 knockout mice**

Supplementary table 2: **Up regulated genes in Xcr1^{+} cDC1 cells from aorta vs spleen, and aorta vs lymph node in ApoE-deficient mice fed a HFD for 20 weeks**

Supplementary table 3: **The top ten high-expressed marker genes in ten clusters**

References

1. Bjorkegren JLM, Lusis AJ. Atherosclerosis: Recent developments. Cell. 2022;185(10):1630-45. doi: 10.1016/j.cell.2022.04.004. PubMed PMID: 35504280; PubMed Central PMCID: PMC9119695.

2. Hansson GK, Hermansson A. The immune system in atherosclerosis. Nat Immunol. 2011;12(3):204-12. Epub 2011/02/16. doi: 10.1038/ni.2001. PubMed PMID: 21321594.

713 3. Lusta KA, Poznyak AV, Sukhorukov VN, Eremin, II, Nadelyaeva, II, Orekhov AN.
714 Hypotheses on Atherogenesis Triggering: Does the Infectious Nature of Atherosclerosis
715 Development Have a Substruction? Cells. 2023;12(5). doi: 10.3390/cells12050707. PubMed
716 PMID: 36899843; PubMed Central PMCID: PMC10001176.
717 4. Hansson GK, Robertson AK, Soderberg-Naucler C. Inflammation and atherosclerosis.
718 Annu Rev Pathol. 2006;1:297-329. Epub 2007/11/28. doi:
719 10.1146/annurev.pathol.1.110304.100100. PubMed PMID: 18039117.
720 5. Hasham SN, Pillarisetti S. Vascular lipases, inflammation and atherosclerosis. Clin Chim
721 Acta. 2006;372(1-2):179-83. Epub 2006/06/13. doi: 10.1016/j.cca.2006.04.020. PubMed PMID:
722 16765928.
723 6. Steinman RM, Hawiger D, Liu K, Bonifaz L, Bonnyay D, Mahnke K, et al. Dendritic cell
724 function in vivo during the steady state: a role in peripheral tolerance. Ann N Y Acad Sci.
725 2003;987:15-25. Epub 2003/05/03. doi: 10.1111/j.1749-6632.2003.tb06029.x. PubMed PMID:
726 12727620.
727 7. Ma-Krupa W, Jeon MS, Spoerl S, Tedder TF, Goronzy JJ, Weyand CM. Activation of
728 arterial wall dendritic cells and breakdown of self-tolerance in giant cell arteritis. J Exp Med.
729 2004;199(2):173-83. Epub 2004/01/22. doi: 10.1084/jem.20030850. PubMed PMID: 14734523;
730 PubMed Central PMCID: PMCPMC2211768.
731 8. Liu P, Yu YR, Spencer JA, Johnson AE, Vallanat CT, Fong AM, et al. CX3CR1 deficiency
732 impairs dendritic cell accumulation in arterial intima and reduces atherosclerotic burden.
733 Arterioscler Thromb Vasc Biol. 2008;28(2):243-50. Epub 2007/12/15. doi:
734 10.1161/ATVBAHA.107.158675. PubMed PMID: 18079406.

735 9. Jongstra-Bilen J, Haidari M, Zhu SN, Chen M, Guha D, Cybulsky MI. Low-grade chronic
736 inflammation in regions of the normal mouse arterial intima predisposed to atherosclerosis. J
737 Exp Med. 2006;203(9):2073-83. Epub 2006/08/09. doi: 10.1084/jem.20060245. PubMed PMID:
738 16894012; PubMed Central PMCID: PMCPMC2118407.
739 10. Bobryshev YV, Lord RS. Ultrastructural recognition of cells with dendritic cell morphology
740 in human aortic intima. Contacting interactions of Vascular Dendritic Cells in athero-resistant
741 and athero-prone areas of the normal aorta. Arch Histol Cytol. 1995;58(3):307-22. Epub
742 1995/08/01. doi: 10.1679/aohc.58.307. PubMed PMID: 8527238.
743 11. Kawahara I, Kitagawa N, Tsutsumi K, Nagata I, Hayashi T, Koji T. The expression of
744 vascular dendritic cells in human atherosclerotic carotid plaques. Hum Pathol.
745 2007;38(9):1378-85. Epub 2007/06/09. doi: 10.1016/j.humpath.2007.02.004. PubMed PMID:
746 17555794.
747 12. Zernecke A, Erhard F, Weinberger T, Schulz C, Ley K, Saliba AE, et al. Integrated
748 single-cell analysis based classification of vascular mononuclear phagocytes in mouse and
749 human atherosclerosis. Cardiovasc Res. 2022. Epub 2022/10/04. doi: 10.1093/cvr/cvac161.
750 PubMed PMID: 36190844.
751 13. Eisenbarth SC. Dendritic cell subsets in T cell programming: location dictates function.
752 Nat Rev Immunol. 2019;19(2):89-103. Epub 2018/11/23. doi: 10.1038/s41577-018-0088-1.
753 PubMed PMID: 30464294; PubMed Central PMCID: PMCPMC7755085.
754 14. Bayerl F, Meiser P, Donakonda S, Hirschberger A, Lacher SB, Pedde AM, et al.
755 Tumor-derived prostaglandin E2 programs cDC1 dysfunction to impair intratumoral
756 orchestration of anti-cancer T cell responses. Immunity. 2023;56(6):1341-58 e11. Epub

757 2023/06/15. doi: 10.1016/j.immuni.2023.05.011. PubMed PMID: 37315536.

758 15. Legein B, Janssen EM, Theelen TL, Gijbels MJ, Walraven J, Klarquist JS, et al. Ablation
759 of CD8alpha(+) dendritic cell mediated cross-presentation does not impact atherosclerosis in
760 hyperlipidemic mice. Scientific reports. 2015;5:15414. Epub 20151021. doi:
761 10.1038/srep15414. PubMed PMID: 26486587; PubMed Central PMCID: PMCPMC4614009.

762 16. Gil-Pulido J, Cochain C, Lippert MA, Schneider N, Butt E, Amezaga N, et al. Deletion of
763 Batf3-dependent antigen-presenting cells does not affect atherosclerotic lesion formation in
764 mice. PLoS One. 2017;12(8):e0181947. Epub 20170803. doi: 10.1371/journal.pone.0181947.
765 PubMed PMID: 28771609; PubMed Central PMCID: PMCPMC5542449.

766 17. Choi JH, Cheong C, Dandamudi DB, Park CG, Rodriguez A, Mehandru S, et al. Flt3
767 signaling-dependent dendritic cells protect against atherosclerosis. Immunity.
768 2011;35(5):819-31. Epub 2011/11/15. doi: 10.1016/j.immuni.2011.09.014. PubMed PMID:
769 22078798.

770 18. Clement M, Haddad Y, Raffort J, Lareyre F, Newland SA, Master L, et al. Deletion of IRF8
771 (Interferon Regulatory Factor 8)-Dependent Dendritic Cells Abrogates Proatherogenic
772 Adaptive Immunity. Circ Res. 2018;122(6):813-20. Epub 2018/02/14. doi:
773 10.1161/CIRCRESAHA.118.312713. PubMed PMID: 29436389.

774 19. Haddad Y, Lahoute C, Clement M, Laurans L, Metghalchi S, Zeboudj L, et al. The
775 Dendritic Cell Receptor DNGR-1 Promotes the Development of Atherosclerosis in Mice. Circ
776 Res. 2017;121(3):234-43. Epub 2017/06/14. doi: 10.1161/CIRCRESAHA.117.310960.
777 PubMed PMID: 28607102.

778 20. Wohn C, Le Guen V, Voluzan O, Fiore F, Henri S, Malissen B. Absence of MHC class II

779 on cDC1 dendritic cells triggers fatal autoimmunity to a cross-presented self-antigen. Sci
780 Immunol. 2020;5(45). Epub 2020/03/15. doi: 10.1126/sciimmunol.aba1896. PubMed PMID:
781 32169954.
782 21. Mundt S, Mrdjen D, Utz SG, Greter M, Schreiner B, Becher B. Conventional DCs sample
783 and present myelin antigens in the healthy CNS and allow parenchymal T cell entry to initiate
784 neuroinflammation. Sci Immunol. 2019;4(31). doi: 10.1126/sciimmunol.aau8380. PubMed
785 PMID: 30679199.
786 22. Robbins CS, Hilgendorf I, Weber GF, Theurl I, Iwamoto Y, Figueiredo JL, et al. Local
787 proliferation dominates lesional macrophage accumulation in atherosclerosis. Nat Med.
788 2013;19(9):1166-72. Epub 2013/08/13. doi: 10.1038/nm.3258. PubMed PMID: 23933982;
789 PubMed Central PMCID: PMCPMC3769444.
790 23. Potteaux S, Gautier EL, Hutchison SB, van Rooijen N, Rader DJ, Thomas MJ, et al.
791 Suppressed monocyte recruitment drives macrophage removal from atherosclerotic plaques
792 of Apoe-/- mice during disease regression. J Clin Invest. 2011;121(5):2025-36. Epub
793 2011/04/21. doi: 10.1172/JCI43802. PubMed PMID: 21505265; PubMed Central PMCID:
794 PMCPMC3083793.
795 24. Yilmaz A, Weber J, Cicha I, Stumpf C, Klein M, Raithel D, et al. Decrease in circulating
796 myeloid dendritic cell precursors in coronary artery disease. J Am Coll Cardiol.
797 2006;48(1):70-80. Epub 2006/07/04. doi: 10.1016/j.jacc.2006.01.078. PubMed PMID:
798 16814651.
799 25. Alberts-Grill N, Denning TL, Rezvan A, Jo H. The role of the vascular dendritic cell
800 network in atherosclerosis. Am J Physiol Cell Physiol. 2013;305(1):C1-21. Epub 2013/04/05.

801 doi: 10.1152/ajpcell.00017.2013. PubMed PMID: 23552284; PubMed Central PMCID:
802 PMCPMC3725520.
803 26. Yan Y, Thakur M, van der Vorst EPC, Weber C, Doring Y. Targeting the chemokine
804 network in atherosclerosis. Atherosclerosis. 2021;330:95-106. Epub 2021/07/13. doi:
805 10.1016/j.atherosclerosis.2021.06.912. PubMed PMID: 34247863.
806 27. Eickhoff S, Brewitz A, Gerner MY, Klauschen F, Komander K, Hemmi H, et al. Robust
807 Anti-viral Immunity Requires Multiple Distinct T Cell-Dendritic Cell Interactions. Cell.
808 2015;162(6):1322-37. Epub 2015/08/25. doi: 10.1016/j.cell.2015.08.004. PubMed PMID:
809 26296422; PubMed Central PMCID: PMCPMC4567961.
810 28. Weber C, Zernecke A, Libby P. The multifaceted contributions of leukocyte subsets to
811 atherosclerosis: lessons from mouse models. Nat Rev Immunol. 2008;8(10):802-15. Epub
812 2008/10/01. doi: 10.1038/nri2415. PubMed PMID: 18825131.
813 29. Worbs T, Hammerschmidt SI, Forster R. Dendritic cell migration in health and disease.
814 Nat Rev Immunol. 2017;17(1):30-48. Epub 2016/11/29. doi: 10.1038/nri.2016.116. PubMed
815 PMID: 27890914.
816 30. Li T, Safitri M, Zhang K, Wang Y, Huang L, Zhu Y, et al. Downregulation of G3BP2
817 reduces atherosclerotic lesions in ApoE(-/-) mice. Atherosclerosis. 2020;310:64-74. Epub
818 2020/09/13. doi: 10.1016/j.atherosclerosis.2020.08.003. PubMed PMID: 32919187.
819 31. Mattiuz R, Wohn C, Ghilas S, Ambrosini M, Alexandre YO, Sanchez C, et al. Novel
820 Cre-Expressing Mouse Strains Permitting to Selectively Track and Edit Type 1 Conventional
821 Dendritic Cells Facilitate Disentangling Their Complexity in vivo. Front Immunol. 2018;9:2805.
822 Epub 2018/12/20. doi: 10.3389/fimmu.2018.02805. PubMed PMID: 30564233; PubMed

823 Central PMCID: PMCPMC6288293.

824 32. Luche H, Weber O, Nageswara Rao T, Blum C, Fehling HJ. Faithful activation of an
825 extra-bright red fluorescent protein in "knock-in" Cre-reporter mice ideally suited for lineage
826 tracing studies. European journal of immunology. 2007;37(1):43-53. Epub 2006/12/16. doi:
827 10.1002/eji.200636745. PubMed PMID: 17171761.

828 33. De Meyer GRY, Zurek M, Puylaert P, Martinet W. Programmed death of macrophages in
829 atherosclerosis: mechanisms and therapeutic targets. Nat Rev Cardiol. 2024. Epub
830 2024/01/02. doi: 10.1038/s41569-023-00957-0. PubMed PMID: 38163815.

831 34. Yu EPK, Reinhold J, Yu H, Starks L, Uryga AK, Foote K, et al. Mitochondrial Respiration
832 Is Reduced in Atherosclerosis, Promoting Necrotic Core Formation and Reducing Relative
833 Fibrous Cap Thickness. Arterioscler Thromb Vasc Biol. 2017;37(12):2322-32. Epub
834 2017/10/04. doi: 10.1161/ATVBAHA.117.310042. PubMed PMID: 28970293; PubMed Central
835 PMCID: PMCPMC5701734.

836 35. Piedrahita JA, Zhang SH, Hagaman JR, Oliver PM, Maeda N. Generation of mice
837 carrying a mutant apolipoprotein E gene inactivated by gene targeting in embryonic stem cells.
838 Proc Natl Acad Sci U S A. 1992;89(10):4471-5. Epub 1992/05/15. doi:
839 10.1073/pnas.89.10.4471. PubMed PMID: 1584779; PubMed Central PMCID:
840 PMCPMC49104.

841 36. Plump AS, Smith JD, Hayek T, Aalto-Setala K, Walsh A, Verstuyft JG, et al. Severe
842 hypercholesterolemia and atherosclerosis in apolipoprotein E-deficient mice created by
843 homologous recombination in ES cells. Cell. 1992;71(2):343-53. Epub 1992/10/16. doi:
844 10.1016/0092-8674(92)90362-g. PubMed PMID: 1423598.

845 37. Fernandez DM, Rahman AH, Fernandez NF, Chudnovskiy A, Amir ED, Amadori L, et al.
846 Single-cell immune landscape of human atherosclerotic plaques. Nat Med.
847 2019;25(10):1576-88. Epub 2019/10/09. doi: 10.1038/s41591-019-0590-4. PubMed PMID:
848 31591603; PubMed Central PMCID: PMCPMC7318784.
849 38. Afek A, Harats D, Roth A, Keren G, George J. Evidence for the involvement of T cell
850 costimulation through the B-7/CD28 pathway in atherosclerotic plaques from apolipoprotein E
851 knockout mice. Exp Mol Pathol. 2004;76(3):219-23. Epub 2004/05/06. doi:
852 10.1016/j.yexmp.2003.12.001. PubMed PMID: 15126104.
853 39. Cancel JC, Crozat K, Dalod M, Mattiuz R. Are Conventional Type 1 Dendritic Cells Critical
854 for Protective Antitumor Immunity and How? Front Immunol. 2019;10:9. Epub 2019/02/28. doi:
855 10.3389/fimmu.2019.00009. PubMed PMID: 30809220; PubMed Central PMCID:
856 PMCPMC6379659.
857 40. Li N, Steiger S, Fei L, Li C, Shi C, Salei N, et al. IRF8-Dependent Type I Conventional
858 Dendritic Cells (cDC1s) Control Post-Ischemic Inflammation and Mildly Protect Against
859 Post-Ischemic Acute Kidney Injury and Disease. Front Immunol. 2021;12:685559. Epub
860 2021/07/09. doi: 10.3389/fimmu.2021.685559. PubMed PMID: 34234783; PubMed Central
861 PMCID: PMCPMC8255684.
862 41. Bottcher JP, Bonavita E, Chakravarty P, Blees H, Cabeza-Cabrerizo M, Sammicheli S, et
863 al. NK Cells Stimulate Recruitment of cDC1 into the Tumor Microenvironment Promoting
864 Cancer Immune Control. Cell. 2018;172(5):1022-37 e14. doi: 10.1016/j.cell.2018.01.004.
865 PubMed PMID: 29429633; PubMed Central PMCID: PMC5847168.
866 42. Dorner BG, Dorner MB, Zhou X, Opitz C, Mora A, Guttler S, et al. Selective expression of

867 the chemokine receptor XCR1 on cross-presenting dendritic cells determines cooperation with
868 CD8+ T cells. Immunity. 2009;31(5):823-33. doi: 10.1016/j.immuni.2009.08.027. PubMed
869 PMID: 19913446.
870 43. Xu F, He D, Ning R, Zeng B, Thompson CW, Li Y, et al. Genetic diversity of chemokine
871 XCL1 and its receptor XCR1 in murine rodents. Developmental and comparative immunology.
872 2019;98:80-8. doi: 10.1016/j.dci.2019.04.008. PubMed PMID: 31026469.
873 44. Yoshida T, Izawa D, Nakayama T, Nakahara K, Kakizaki M, Imai T, et al. Molecular
874 cloning of mXCR1, the murine SCM-1/lymphotactin receptor. FEBS letters. 1999;458(1):37-40.
875 doi: 10.1016/s0014-5793(99)01114-x. PubMed PMID: 10518929.
876 45. Tall AR, Bornfeldt KE. Inflammasomes and Atherosclerosis: a Mixed Picture. Circ Res.
877 2023;132(11):1505-20. doi: 10.1161/CIRCRESAHA.123.321637. PubMed PMID: 37228237;
878 PubMed Central PMCID: PMC10213995.
879 46. Vallejo J, Cochain C, Zernecke A, Ley K. Heterogeneity of immune cells in human
880 atherosclerosis revealed by scRNA-Seq. Cardiovasc Res. 2021;117(13):2537-43. doi:
881 10.1093/cvr/cvab260. PubMed PMID: 34343272; PubMed Central PMCID: PMC8921647.
882 47. Guo X, Zhou Y, Wu T, Zhu X, Lai W, Wu L. Generation of mouse and human dendritic
883 cells in vitro. J Immunol Methods. 2016;432:24-9. Epub 2016/02/16. doi:
884 10.1016/j.jim.2016.02.011. PubMed PMID: 26876301.
885 48. Anselmi G, Helft J, Guermonprez P. Development and function of human dendritic cells in
886 humanized mice models. Mol Immunol. 2020;125:151-61. Epub 2020/07/21. doi:
887 10.1016/j.molimm.2020.07.005. PubMed PMID: 32688117.
888 49. Blanco P, Palucka AK, Pascual V, Banchereau J. Dendritic cells and cytokines in human

889 inflammatory and autoimmune diseases. Cytokine Growth Factor Rev. 2008;19(1):41-52.
890 Epub 2008/02/09. doi: 10.1016/j.cytogfr.2007.10.004. PubMed PMID: 18258476; PubMed
891 Central PMCID: PMCPMC2413068.
892 50. Steinman RM. Dendritic cells: understanding immunogenicity. European journal of
893 immunology. 2007;37 Suppl 1:S53-60. Epub 2007/11/01. doi: 10.1002/eji.200737400.
894 PubMed PMID: 17972346.
895 51. Steinman RM, Adams JC, Cohn ZA. Identification of a novel cell type in peripheral
896 lymphoid organs of mice. IV. Identification and distribution in mouse spleen. J Exp Med.
897 1975;141(4):804-20. Epub 1975/04/01. PubMed PMID: 1127378; PubMed Central PMCID:
898 PMCPMC2189754.
899 52. Steinman RM, Kaplan G, Witmer MD, Cohn ZA. Identification of a novel cell type in
900 peripheral lymphoid organs of mice. V. Purification of spleen dendritic cells, new surface
901 markers, and maintenance in vitro. J Exp Med. 1979;149(1):1-16. Epub 1979/01/01. doi:
902 10.1084/jem.149.1.1. PubMed PMID: 762493; PubMed Central PMCID: PMCPMC2184752.
903 53. Clark GJ, Silveira PA, Hogarth PM, Hart DNJ. The cell surface phenotype of human
904 dendritic cells. Semin Cell Dev Biol. 2019;86:3-14. Epub 2018/03/03. doi:
905 10.1016/j.semcdb.2018.02.013. PubMed PMID: 29499385.
906 54. Brewitz A, Eickhoff S, Dahling S, Quast T, Bedoui S, Kroczek RA, et al. CD8(+) T Cells
907 Orchestrate pDC-XCR1(+) Dendritic Cell Spatial and Functional Cooperativity to Optimize
908 Priming. Immunity. 2017;46(2):205-19. Epub 2017/02/14. doi: 10.1016/j.immuni.2017.01.003.
909 PubMed PMID: 28190711; PubMed Central PMCID: PMCPMC5362251.
910 55. Alexandre YO, Ghilas S, Sanchez C, Le Bon A, Crozat K, Dalod M. XCR1+ dendritic cells

911 promote memory CD8+ T cell recall upon secondary infections with Listeria monocytogenes or
912 certain viruses. J Exp Med. 2016;213(1):75-92. Epub 2015/12/24. doi: 10.1084/jem.20142350.
913 PubMed PMID: 26694969; PubMed Central PMCID: PMCPMC4710197.
914 56. Domenjo-Vila E, Casella V, Iwabuchi R, Fossum E, Pedragosa M, Castellvi Q, et al.
915 XCR1+ DCs are critical for T cell-mediated immunotherapy of chronic viral infections. Cell Rep.
916 2023;42(2):112123. Epub 2023/02/17. doi: 10.1016/j.celrep.2023.112123. PubMed PMID:
917 36795562.
918 57. Deczkowska A, David E, Ramadori P, Pfister D, Safran M, Li B, et al. XCR1(+) type 1
919 conventional dendritic cells drive liver pathology in non-alcoholic steatohepatitis. Nat Med.
920 2021;27(6):1043-54. Epub 2021/05/22. doi: 10.1038/s41591-021-01344-3. PubMed PMID:
921 34017133.
922 58. Mysore V, Tahir S, Furuhashi K, Arora J, Rosetti F, Cullere X, et al. Monocytes transition
923 to macrophages within the inflamed vasculature via monocyte CCR2 and endothelial TNFR2.
924 J Exp Med. 2022;219(5). Epub 2022/04/12. doi: 10.1084/jem.20210562. PubMed PMID:
925 35404389; PubMed Central PMCID: PMCPMC9006314.
926 59. Liu Z, Liao F, Zhu J, Zhou D, Heo GS, Leuhmann HP, et al. Reprogramming alveolar
927 macrophage responses to TGF-beta reveals CCR2+ monocyte activity that promotes
928 bronchiolitis obliterans syndrome. J Clin Invest. 2022;132(19). Epub 2022/10/04. doi:
929 10.1172/JCI159229. PubMed PMID: 36189800; PubMed Central PMCID: PMCPMC9525120.
930 60. Kim D, An L, Moon J, Maymi VI, McGurk AI, Rudd BD, et al. Ccr2+ Monocyte-Derived
931 Macrophages Influence Trajectories of Acquired Therapy Resistance in Braf-Mutant
932 Melanoma. Cancer Res. 2023;83(14):2328-44. Epub 2023/05/17. doi:

933 10.1158/0008-5472.CAN-22-2841. PubMed PMID: 37195124; PubMed Central PMCID:
934 PMCPMC10478295.
935 61. Inui H, Nishida M, Ichii M, Nakaoka H, Asaji M, Ide S, et al. XCR1(+) conventional
936 dendritic cell-induced CD4(+) T helper 1 cell activation exacerbates cardiac remodeling after
937 ischemic myocardial injury. J Mol Cell Cardiol. 2023;176:68-83. Epub 2023/02/06. doi:
938 10.1016/j.yjmcc.2023.01.011. PubMed PMID: 36739942.
939 62. Moore KJ, Tabas I. Macrophages in the pathogenesis of atherosclerosis. Cell.
940 2011;145(3):341-55. Epub 2011/05/03. doi: 10.1016/j.cell.2011.04.005. PubMed PMID:
941 21529710; PubMed Central PMCID: PMCPMC3111065.
942 63. Yoshida T, Imai T, Kakizaki M, Nishimura M, Takagi S, Yoshie O. Identification of single C
943 motif-1/lymphotactin receptor XCR1. The Journal of biological chemistry.
944 1998;273(26):16551-4. doi: 10.1074/jbc.273.26.16551. PubMed PMID: 9632725.
945 64. Chu VT, Weber T, Graf R, Sommermann T, Petsch K, Sack U, et al. Efficient generation
946 of Rosa26 knock-in mice using CRISPR/Cas9 in C57BL/6 zygotes. BMC biotechnology.
947 2016;16:4. doi: 10.1186/s12896-016-0234-4. PubMed PMID: 26772810; PubMed Central
948 PMCID: PMC4715285.
949 65. Larson MA. Pronuclear Microinjection of One-Cell Embryos. Methods in molecular biology.
950 2020;2066:27-33. doi: 10.1007/978-1-4939-9837-1_2. PubMed PMID: 31512204.
951 66. Voisinne G, Kersse K, Chaoui K, Lu L, Chaix J, Zhang L, et al. Quantitative interactomics
952 in primary T cells unveils TCR signal diversification extent and dynamics. Nat Immunol.
953 2019;20(11):1530-41. Epub 2019/10/09. doi: 10.1038/s41590-019-0489-8. PubMed PMID:
954 31591574; PubMed Central PMCID: PMCPMC6859066.

955 67. Huang R, Guo G, Lu L, Fu R, Luo J, Liu Z, et al. The three members of the Vav family
956 proteins form complexes that concur to foam cell formation and atherosclerosis. Journal of
957 lipid research. 2019;60(12):2006-19. doi: 10.1194/jlr.M094771. PubMed PMID: 31570505;
958 PubMed Central PMCID: PMC6889716.
959

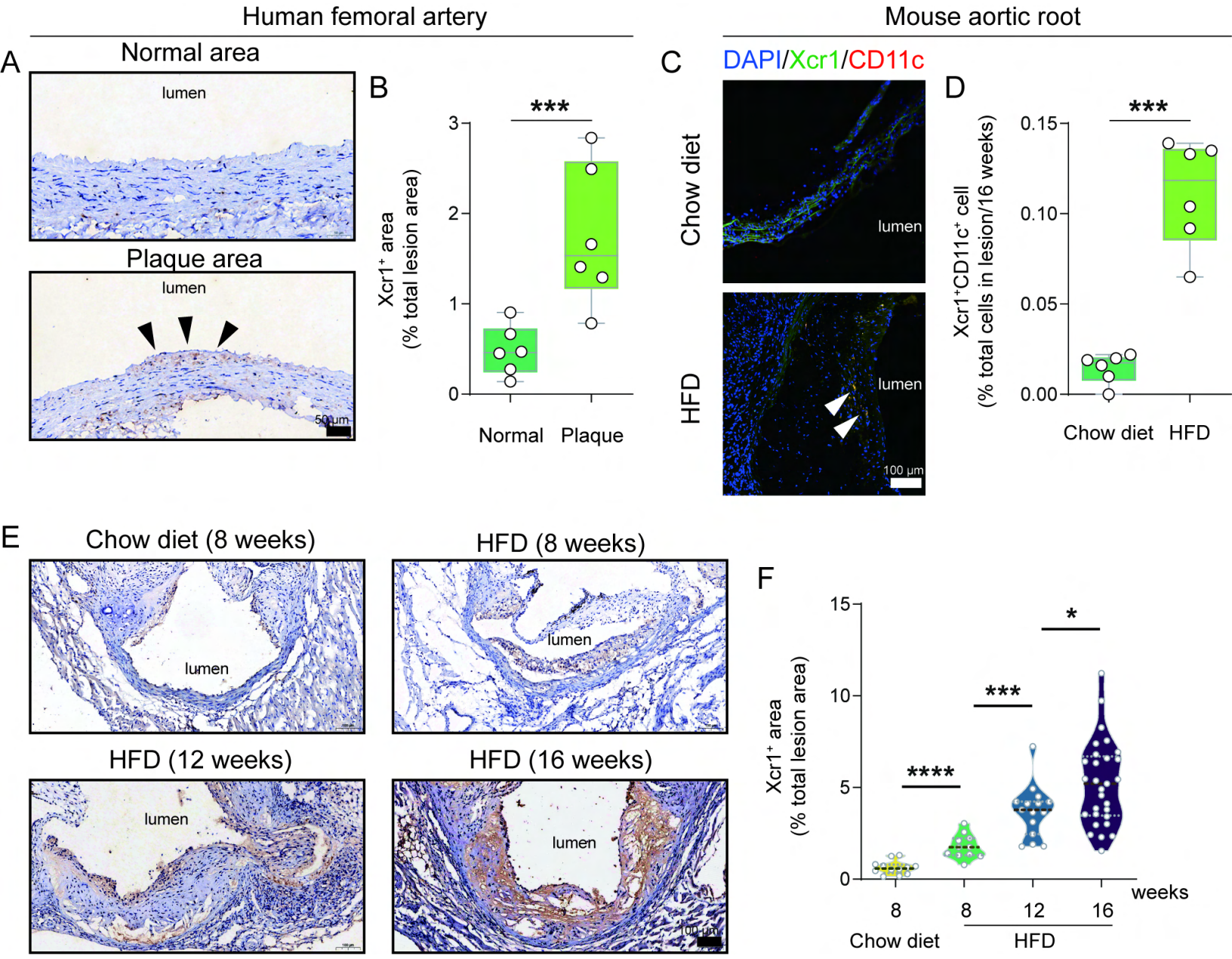
Human femoral artery
Mouse aortic root
A
Normal area
lumen
Plaque area
lumen
500 µm
B
***
Xcr1⁺ area
(% total lesion area)
3
2
1
0
Normal
Plaque
C
DAPI/Xcr1/CD11c
Chow diet
HFD
lumen
lumen
100 µm
D
***
Xcr1⁺CD11c⁺ cell
(% total cells in lesion/16 weeks)
0.15
0.10
0.05
0.00
Chow diet
HFD
E
Chow diet (8 weeks)
lumen
HFD (8 weeks)
lumen
HFD (12 weeks)
lumen
HFD (16 weeks)
lumen
100 µm
F
*
***
****
Xcr1⁺ area
(% total lesion area)
15
10
5
0
weeks
8
8
12
16
Chow diet
HFD

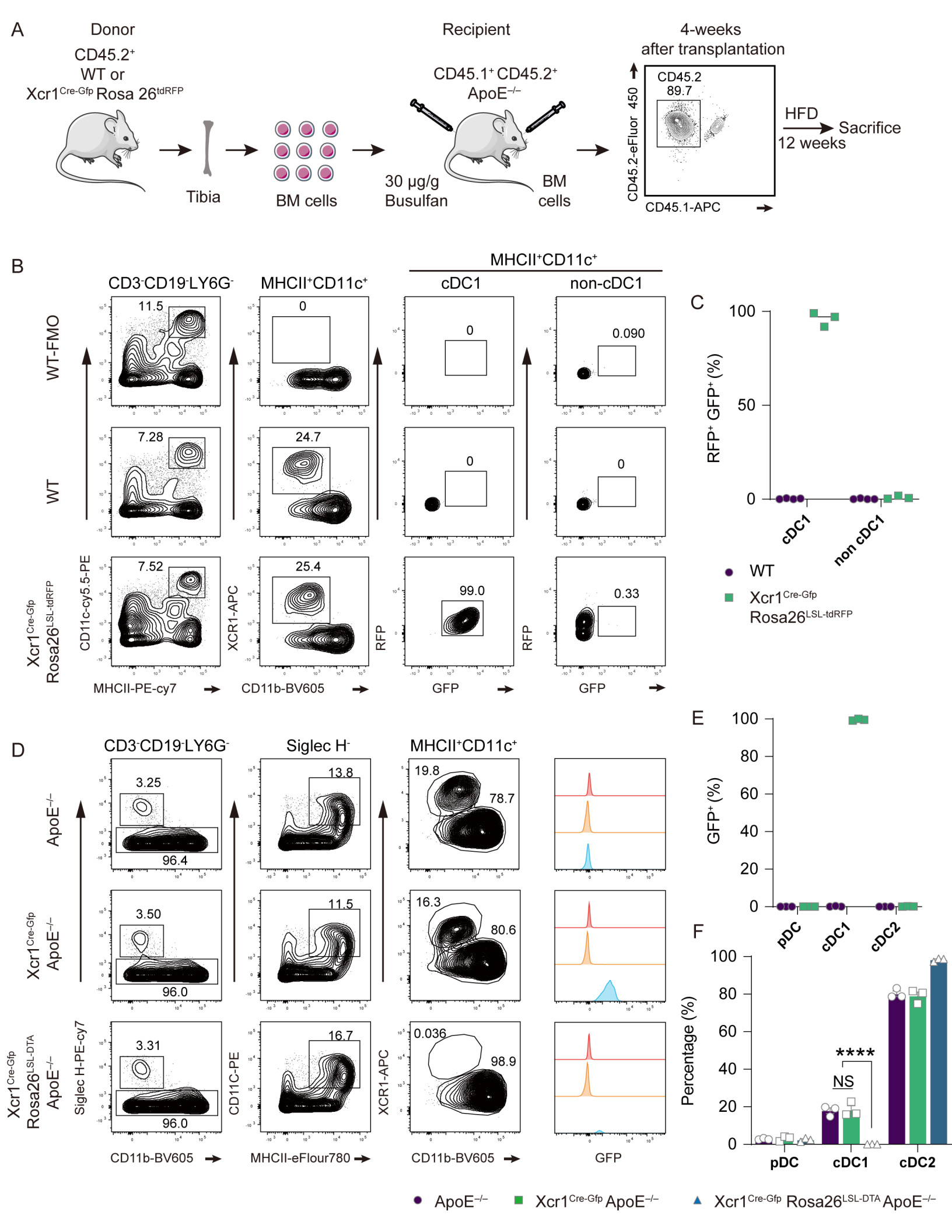
A
Donor
CD45.2+
WT or
Xcr1Cre-Gfp Rosa 26tdRFP
Tibia
BM cells
Recipient
CD45.1+ CD45.2+
ApoE−/−
30 µg/g
Busulfan
BM
cells
4-weeks
after transplantation
CD45.2
89.7
CD45.2-eFluor 450
CD45.1-APC
HFD
12 weeks
Sacrifice
B
MHCII+CD11c+
CD3-CD19-LY6G-
MHCII+CD11c+
cDC1
non-cDC1
WT-FMO
WT
Xcr1Cre-Gfp
Rosa26LSL-tdRFP
11.5
0
0
0.090
7.28
24.7
0
0
7.52
25.4
99.0
0.33
CD11c-cy5.5-PE
XCR1-APC
RFP
RFP
MHCII-PE-cy7
CD11b-BV605
GFP
GFP
C
RFP+ GFP+ (%)
100
50
0
cDC1
non cDC1
WT
Xcr1Cre-Gfp
Rosa26LSL-tdRFP
D
CD3-CD19-LY6G-
Siglec H-
MHCII+CD11c+
ApoE−/−
Xcr1Cre-Gfp
ApoE−/−
Xcr1Cre-Gfp
Rosa26LSL-DTA
ApoE−/−
3.25
96.4
13.8
19.8
78.7
3.50
96.0
11.5
16.3
80.6
3.31
96.0
16.7
0.036
98.9
Siglec H-PE-cy7
CD11C-PE
XCR1-APC
CD11b-BV605
MHCII-eFlour780
CD11b-BV605
GFP
E
GFP+ (%)
100
80
60
40
20
0
pDC
cDC1
cDC2
F
Percentage (%)
100
80
60
40
20
0
****
NS
pDC
cDC1
cDC2
ApoE−/−
Xcr1Cre-Gfp ApoE−/−
Xcr1Cre-Gfp Rosa26LSL-DTA ApoE−/−

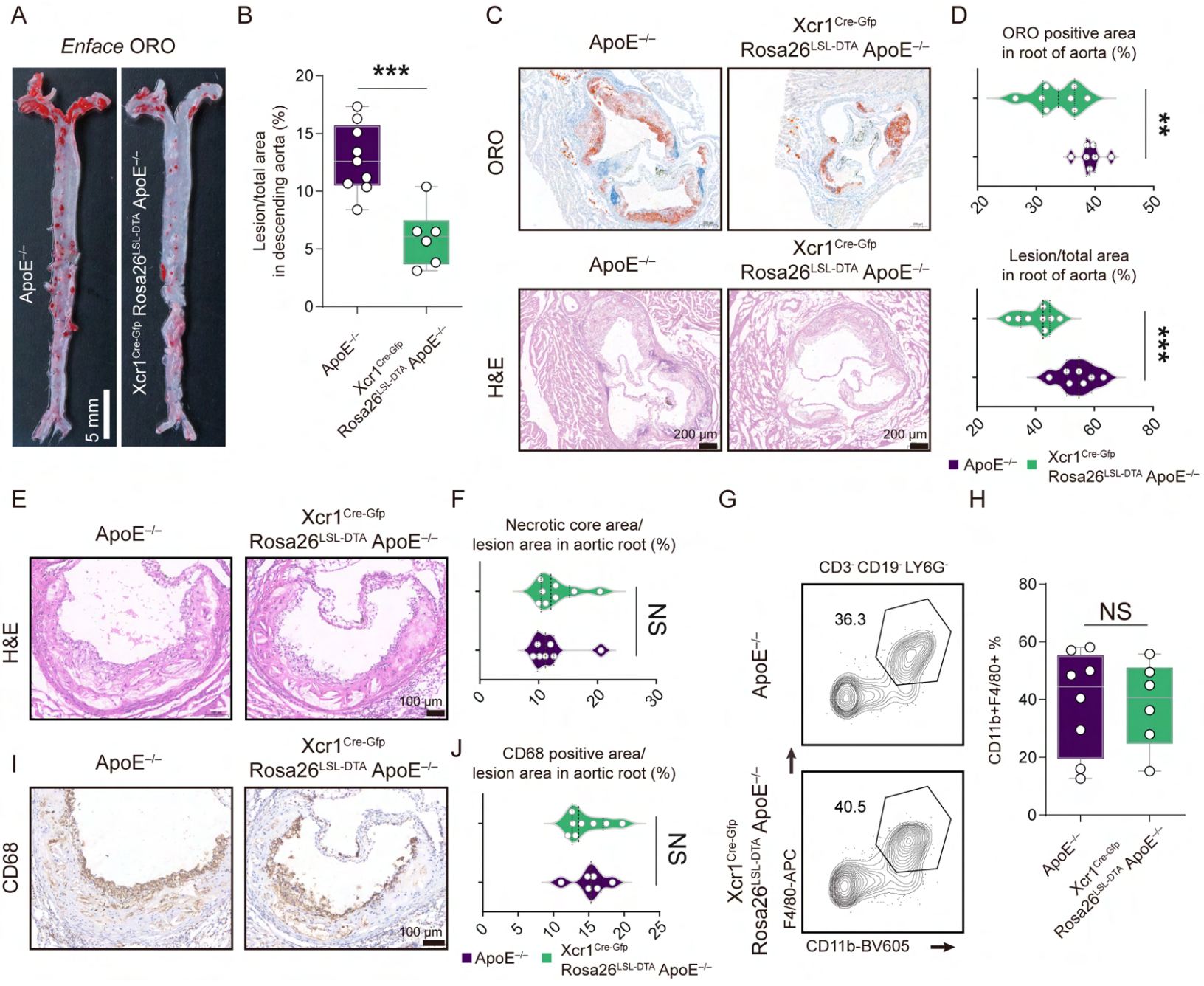
A
Enface ORO
ApoE−/−
Xcr1Cre-Gfp Rosa26LSL-DTA ApoE−/−
5 mm
B
***
Lesion/total area in descending aorta (%)
ApoE−/−
Xcr1Cre-Gfp Rosa26LSL-DTA ApoE−/−
C
ORO
H&E
200 µm
D
ORO positive area in root of aorta (%)
**
Lesion/total area in root of aorta (%)
***
E
100 µm
F
Necrotic core area/ lesion area in aortic root (%)
NS
G
CD3- CD19- LY6G-
36.3
40.5
F4/80-APC
CD11b-BV605
H
CD11b+F4/80+ %
NS
I
CD68
J
CD68 positive area/ lesion area in aortic root (%)

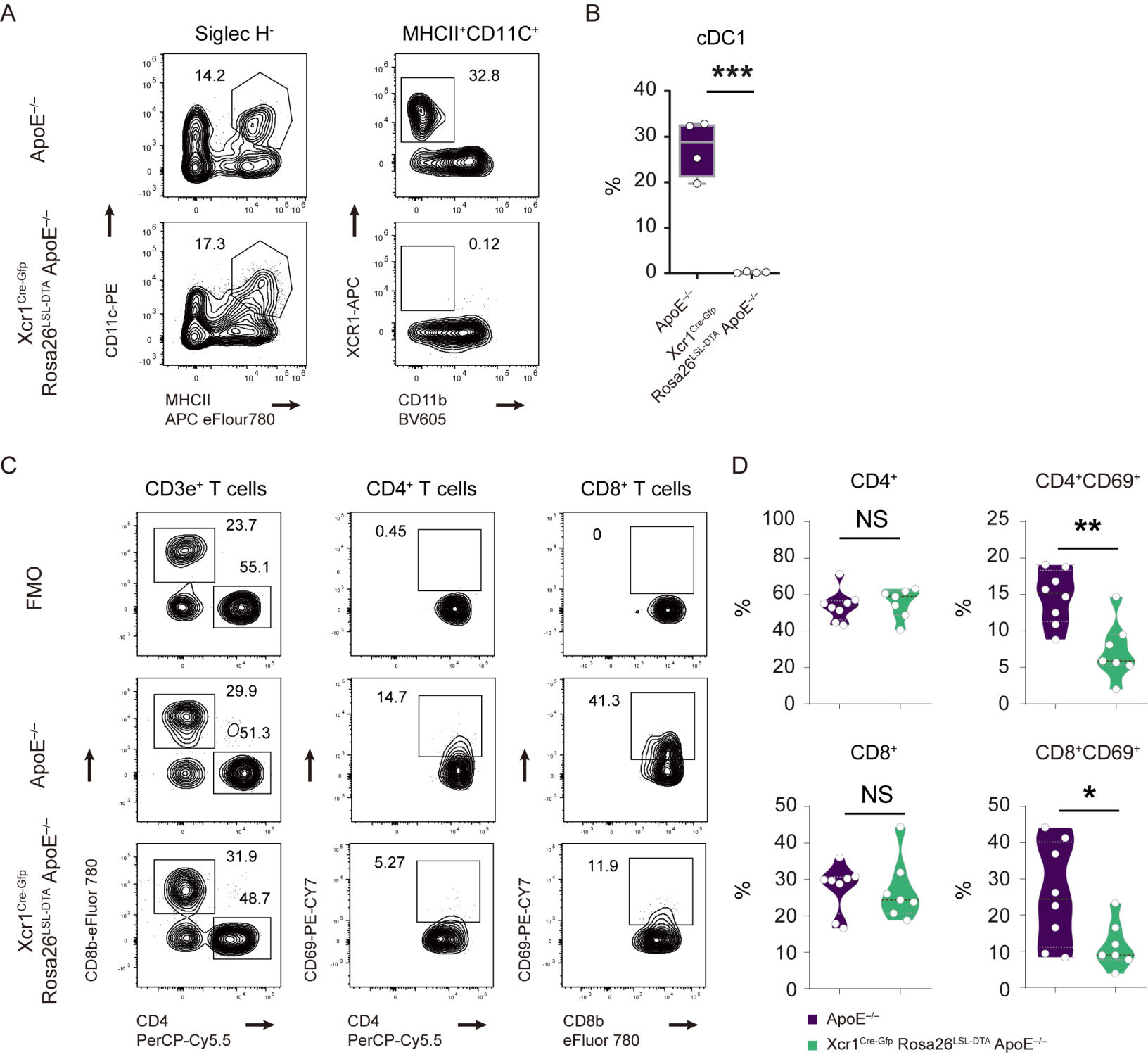
A
Siglec H-
MHCII+CD11C+
ApoE−/−
Xcr1Cre-Gfp Rosa26LSL-DTA ApoE−/−
14.2
32.8
17.3
0.12
CD11c-PE
XCR1-APC
MHCII
APC eFlour780
CD11b
BV605
B
cDC1
***
%
ApoE−/−
Xcr1Cre-Gfp Rosa26LSL-DTA ApoE−/−
C
CD3e+ T cells
CD4+ T cells
CD8+ T cells
FMO
23.7
55.1
0.45
0
29.9
51.3
14.7
41.3
31.9
48.7
5.27
11.9
CD8b-eFluor 780
CD69-PE-CY7
CD4
PerCP-Cy5.5
CD8b
eFluor 780
D
CD4+
CD4+CD69+
CD8+
CD8+CD69+
NS
**
*
ApoE−/−
Xcr1Cre-Gfp Rosa26LSL-DTA ApoE−/−

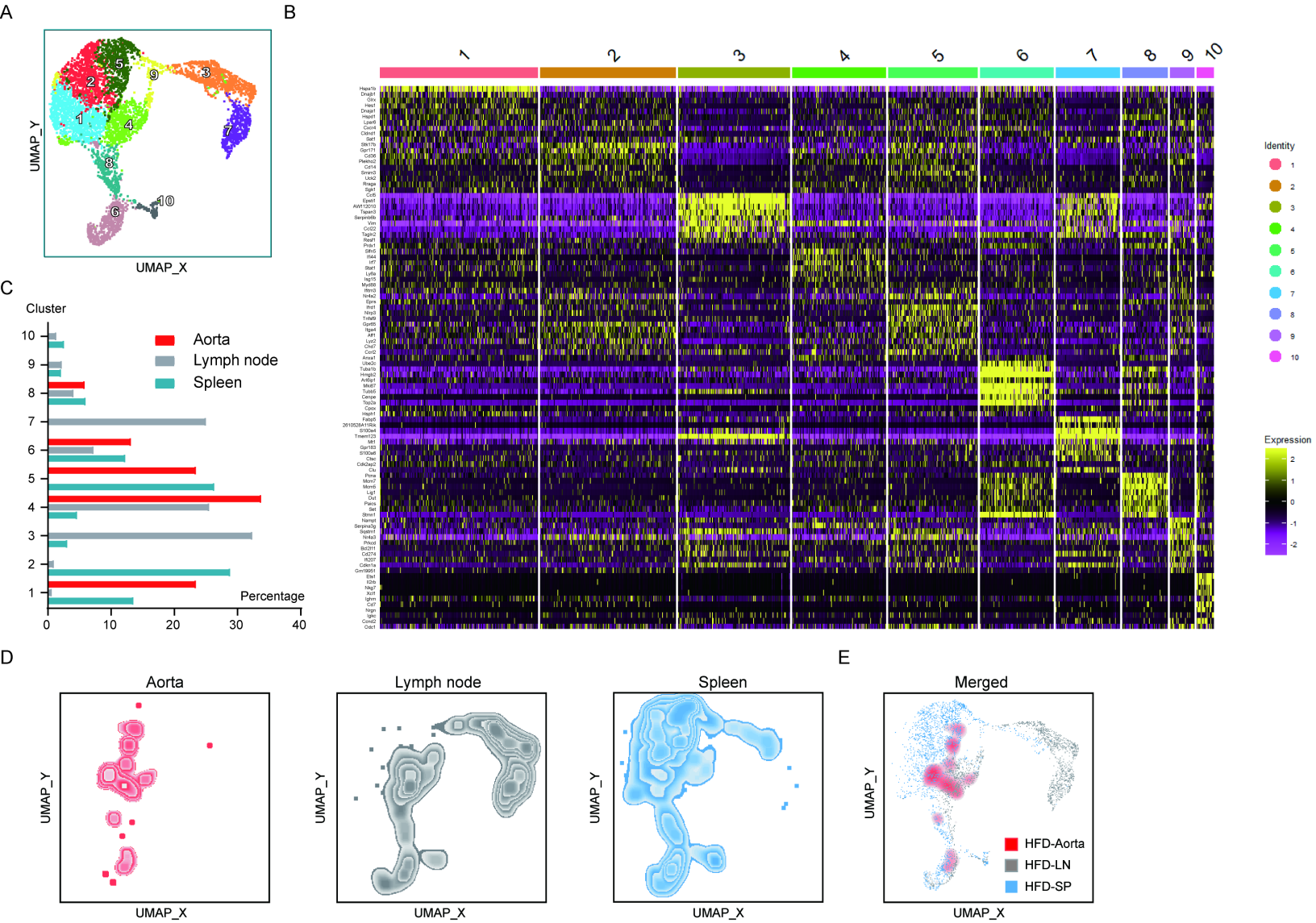
A
UMAP_Y
UMAP_X
B
Identity
Expression
C
Cluster
Aorta
Lymph node
Spleen
Percentage
D
Aorta
Lymph node
Spleen
E
Merged
HFD-Aorta
HFD-LN
HFD-SP

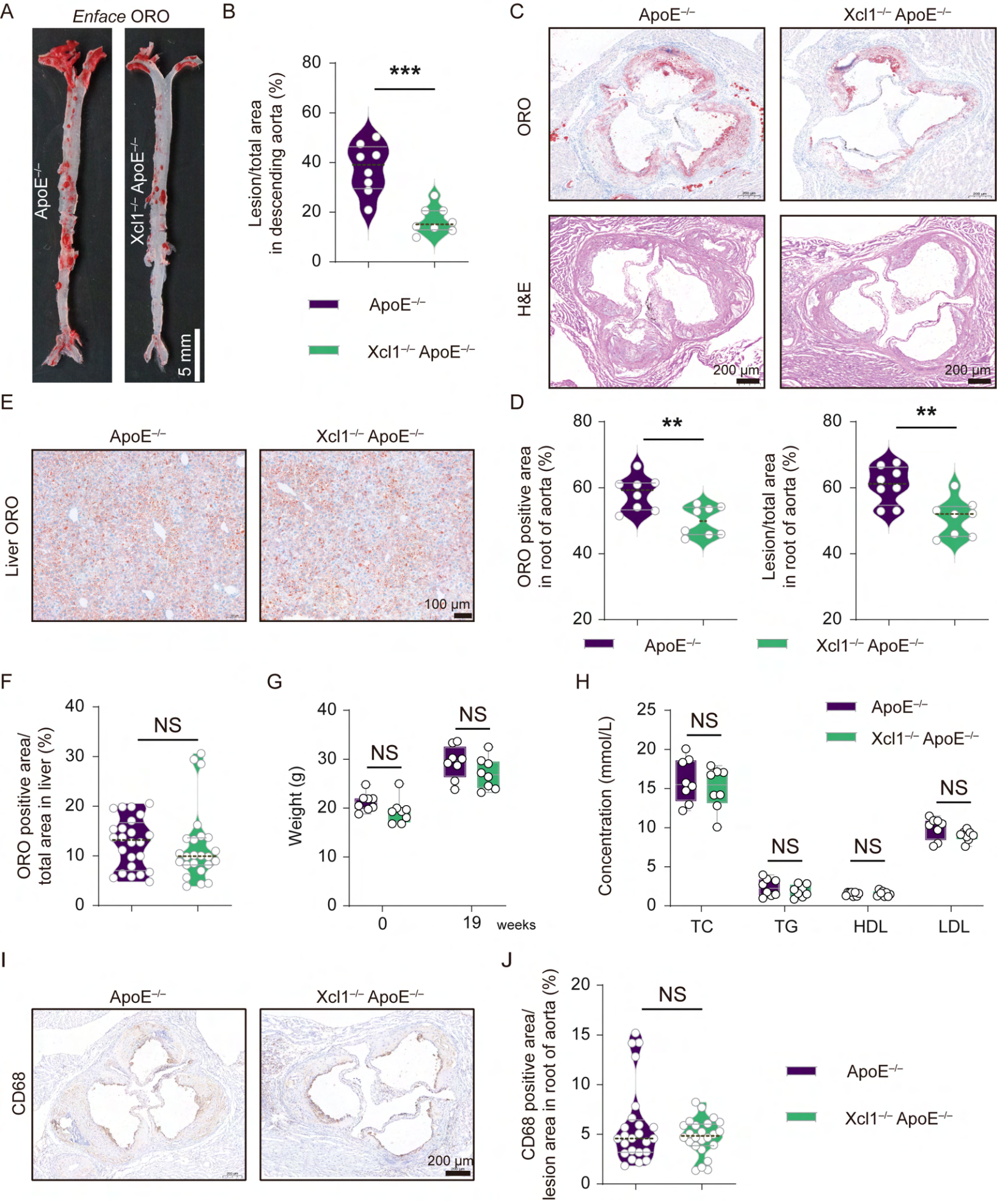
A
Enface ORO
ApoE−/−
Xcl1−/− ApoE−/−
5 mm
B
Lesion/total area in descending aorta (%)
***
ApoE−/−
Xcl1−/− ApoE−/−
C
ApoE−/−
Xcl1−/− ApoE−/−
ORO
H&E
200 µm
200 µm
E
ApoE−/−
Xcl1−/− ApoE−/−
Liver ORO
100 µm
D
ORO positive area in root of aorta (%)
**
Lesion/total area in root of aorta (%)
**
ApoE−/−
Xcl1−/− ApoE−/−
F
ORO positive area/ total area in liver (%)
NS
G
Weight (g)
NS
NS
0
19
weeks
H
Concentration (mmol/L)
NS
NS
NS
NS
TC
TG
HDL
LDL
ApoE−/−
Xcl1−/− ApoE−/−
I
ApoE−/−
Xcl1−/− ApoE−/−
CD68
200 µm
J
CD68 positive area/ lesion area in root of aorta (%)
NS
ApoE−/−
Xcl1−/− ApoE−/−

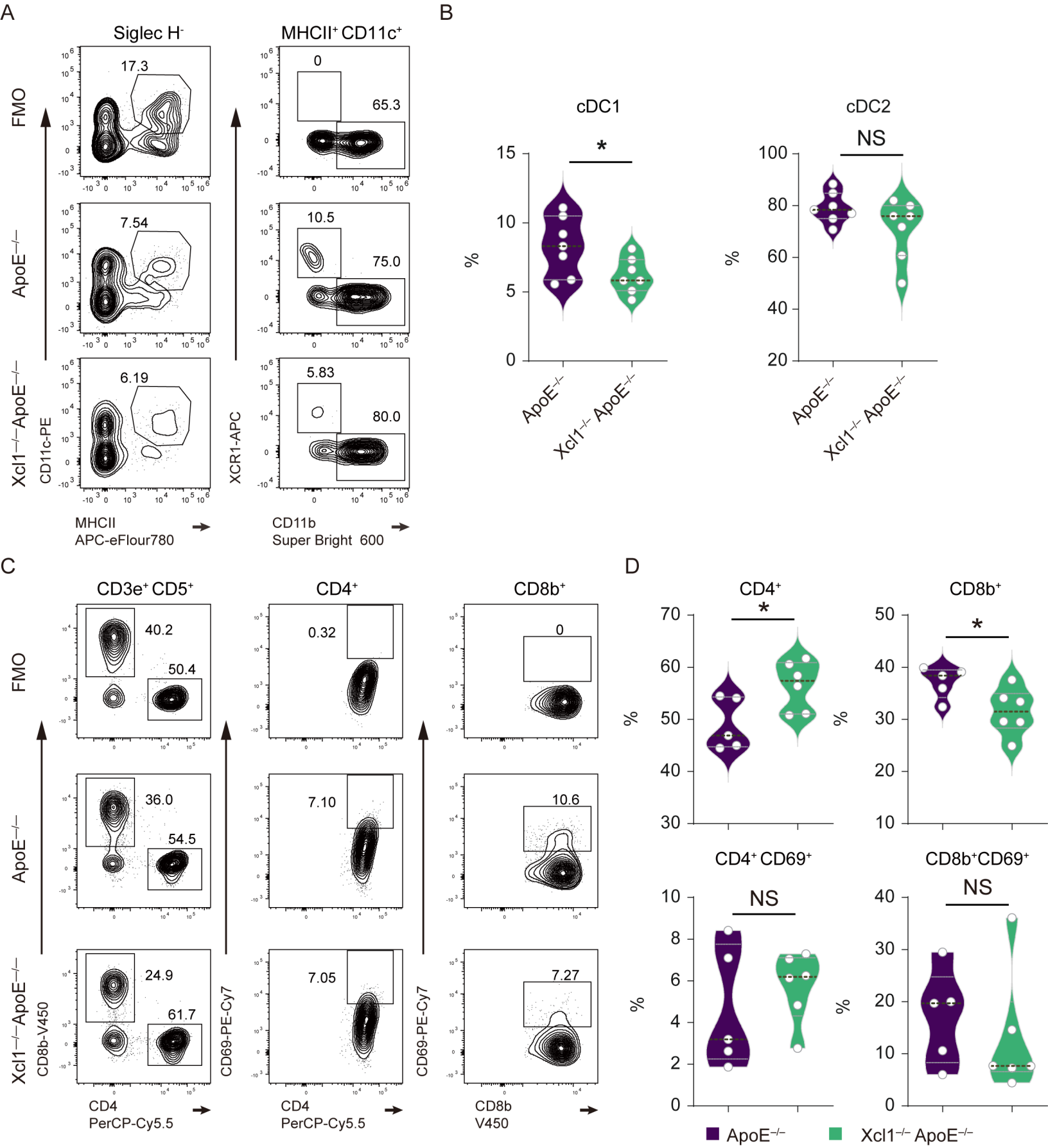
A
Siglec H-
MHCII+ CD11c+
FMO
ApoE−/−
Xcl1−/− ApoE−/−
17.3
7.54
6.19
0
65.3
10.5
75.0
5.83
80.0
CD11c-PE
XCR1-APC
MHCII
APC-eFlour780
CD11b
Super Bright 600
B
cDC1
cDC2
*
NS
%
ApoE−/−
Xcl1−/− ApoE−/−
C
CD3e+ CD5+
CD4+
CD8b+
40.2
50.4
36.0
54.5
24.9
61.7
0.32
7.10
7.05
0
10.6
7.27
CD8b-V450
CD69-PE-Cy7
CD4
PerCP-Cy5.5
CD8b
V450
D
CD4+
CD8b+
CD4+ CD69+
CD8b+CD69+
*
NS
%
ApoE−/−
Xcl1−/− ApoE−/−

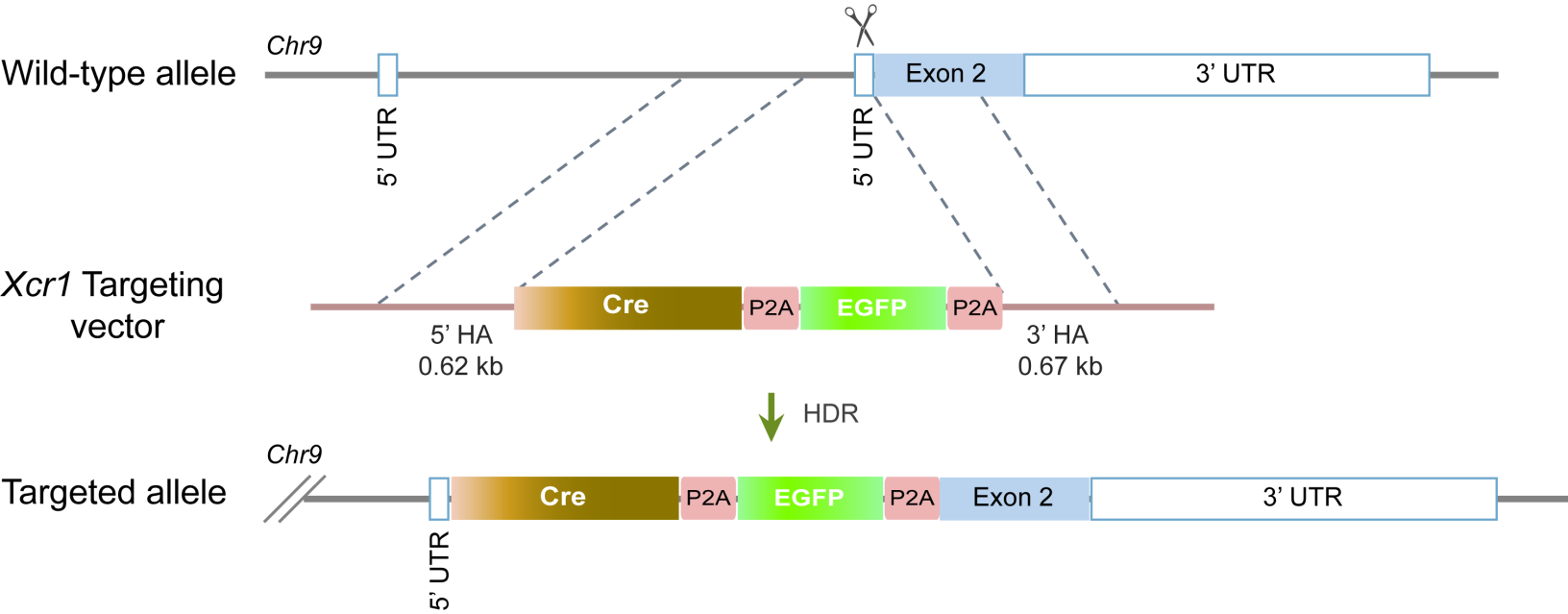
Wild-type allele
Chr9
5' UTR
5' UTR
Exon 2
3' UTR
Xcr1 Targeting vector
Cre
P2A
EGFP
P2A
5' HA
0.62 kb
3' HA
0.67 kb
HDR
Targeted allele
Chr9
Cre
P2A
EGFP
P2A
Exon 2
3' UTR
5' UTR

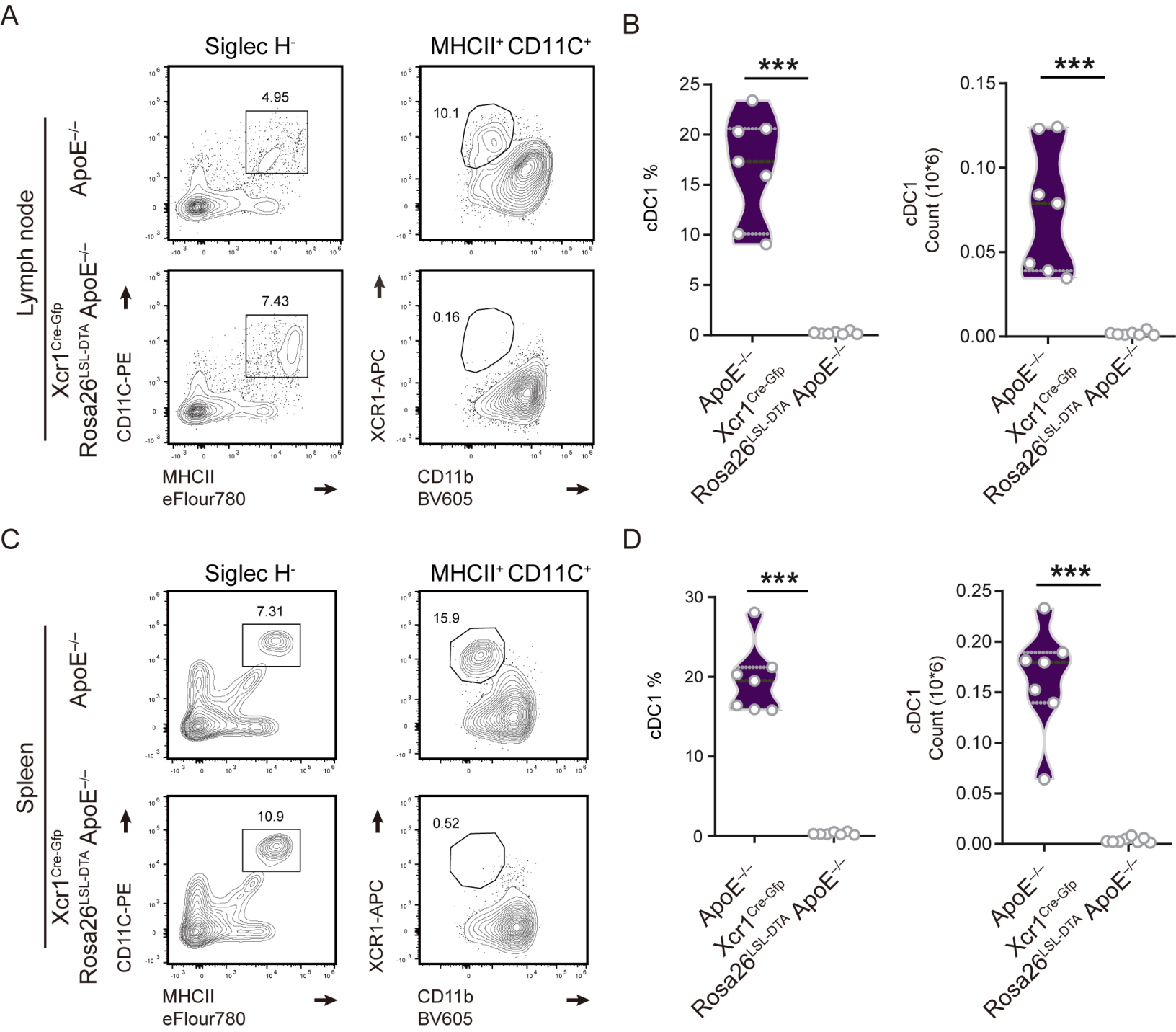
A
Siglec H-
MHCII+ CD11C+
Lymph node
ApoE−/−
Xcr1Cre-Gfp ApoE−/−
Rosa26LSL-DTA
4.95
10.1
7.43
0.16
CD11C-PE
XCR1-APC
MHCII
eFlour780
CD11b
BV605
B
***
cDC1 %
cDC1
Count (10*6)
ApoE−/−
Xcr1Cre-Gfp
Rosa26LSL-DTA ApoE−/−
C
Siglec H-
MHCII+ CD11C+
Spleen
ApoE−/−
Xcr1Cre-Gfp ApoE−/−
Rosa26LSL-DTA
7.31
15.9
10.9
0.52
CD11C-PE
XCR1-APC
MHCII
eFlour780
CD11b
BV605
D
***
cDC1 %
cDC1
Count (10*6)
ApoE−/−
Xcr1Cre-Gfp
Rosa26LSL-DTA ApoE−/−

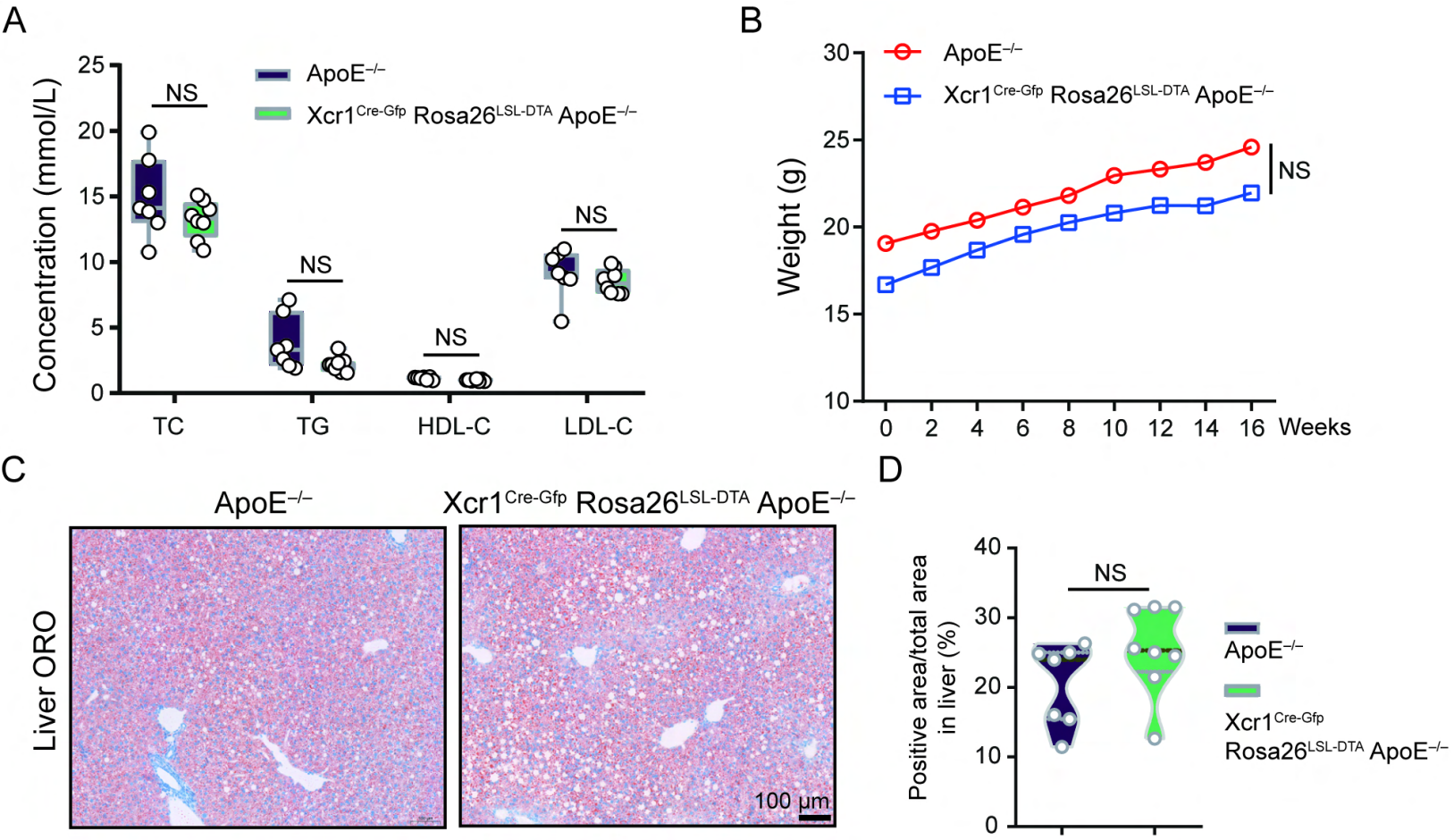
A
Concentration (mmol/L)
25
20
15
10
5
0
NS
NS
NS
NS
TC
TG
HDL-C
LDL-C
ApoE−/−
Xcr1Cre-Gfp Rosa26LSL-DTA ApoE−/−
B
Weight (g)
30
25
20
15
10
0
2
4
6
8
10
12
14
16
Weeks
NS
ApoE−/−
Xcr1Cre-Gfp Rosa26LSL-DTA ApoE−/−
C
ApoE−/−
Xcr1Cre-Gfp Rosa26LSL-DTA ApoE−/−
Liver ORO
100 μm
D
Positive area/total area in liver (%)
40
30
20
10
0
NS
ApoE−/−
Xcr1Cre-Gfp Rosa26LSL-DTA ApoE−/−

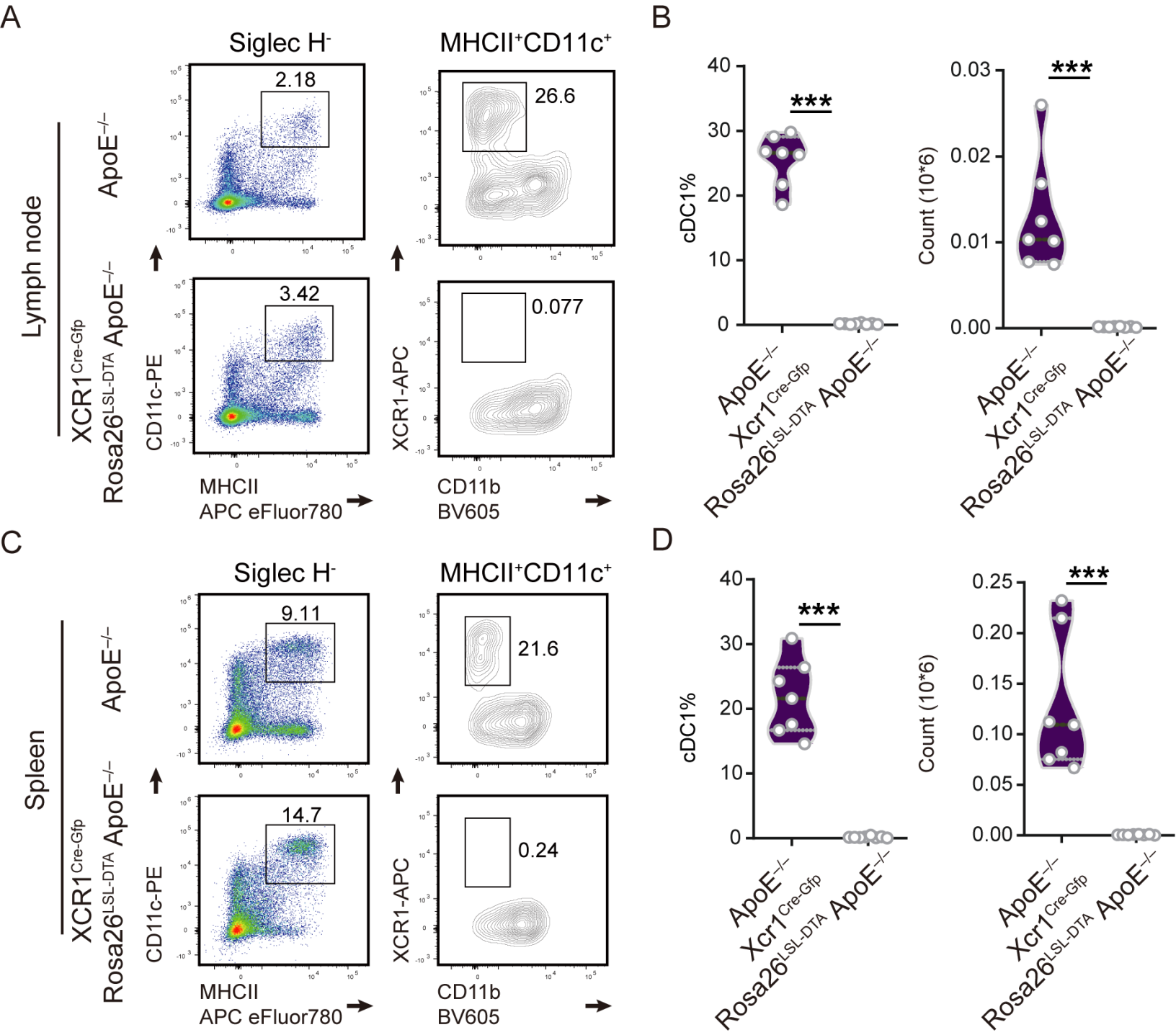
A
Siglec H-
MHCII+CD11c+
Lymph node
ApoE−/−
XCR1Cre-Gfp ApoE−/−
Rosa26LSL-DTA
2.18
26.6
3.42
0.077
CD11c-PE
XCR1-APC
MHCII
APC eFluor780
CD11b
BV605
B
cDC1%
Count (10*6)
***
***
ApoE−/−
Xcr1Cre-Gfp
Rosa26LSL-DTA
ApoE−/−
C
Siglec H-
MHCII+CD11c+
Spleen
ApoE−/−
XCR1Cre-Gfp ApoE−/−
Rosa26LSL-DTA
9.11
21.6
14.7
0.24
CD11c-PE
XCR1-APC
MHCII
APC eFluor780
CD11b
BV605
D
cDC1%
Count (10*6)
***
***
ApoE−/−
Xcr1Cre-Gfp
Rosa26LSL-DTA
ApoE−/−

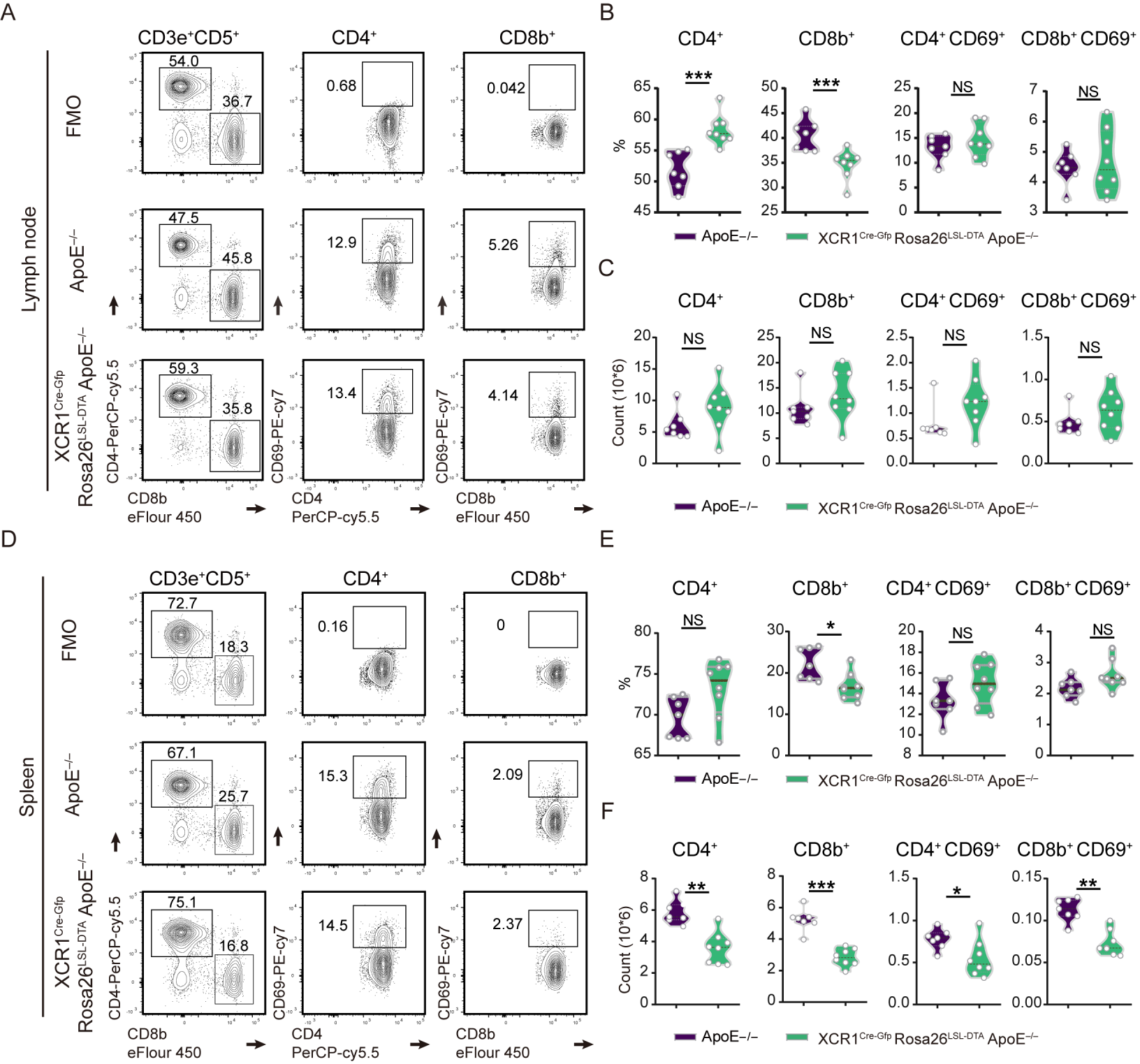
A
B
C
D
E
F
Lymph node
Spleen
FMO
ApoE−/−
XCR1Cre-Gfp Rosa26LSL-DTA ApoE−/−
CD3e+CD5+
CD4+
CD8b+
CD4+ CD69+
CD8b+ CD69+
54.0
36.7
0.68
0.042
47.5
45.8
12.9
5.26
59.3
35.8
13.4
4.14
72.7
18.3
0.16
0
67.1
25.7
15.3
2.09
75.1
16.8
14.5
2.37
CD4-PerCP-cy5.5
CD69-PE-cy7
CD8b eFlour 450
CD4 PerCP-cy5.5
%
Count (10*6)
***
**
*
NS

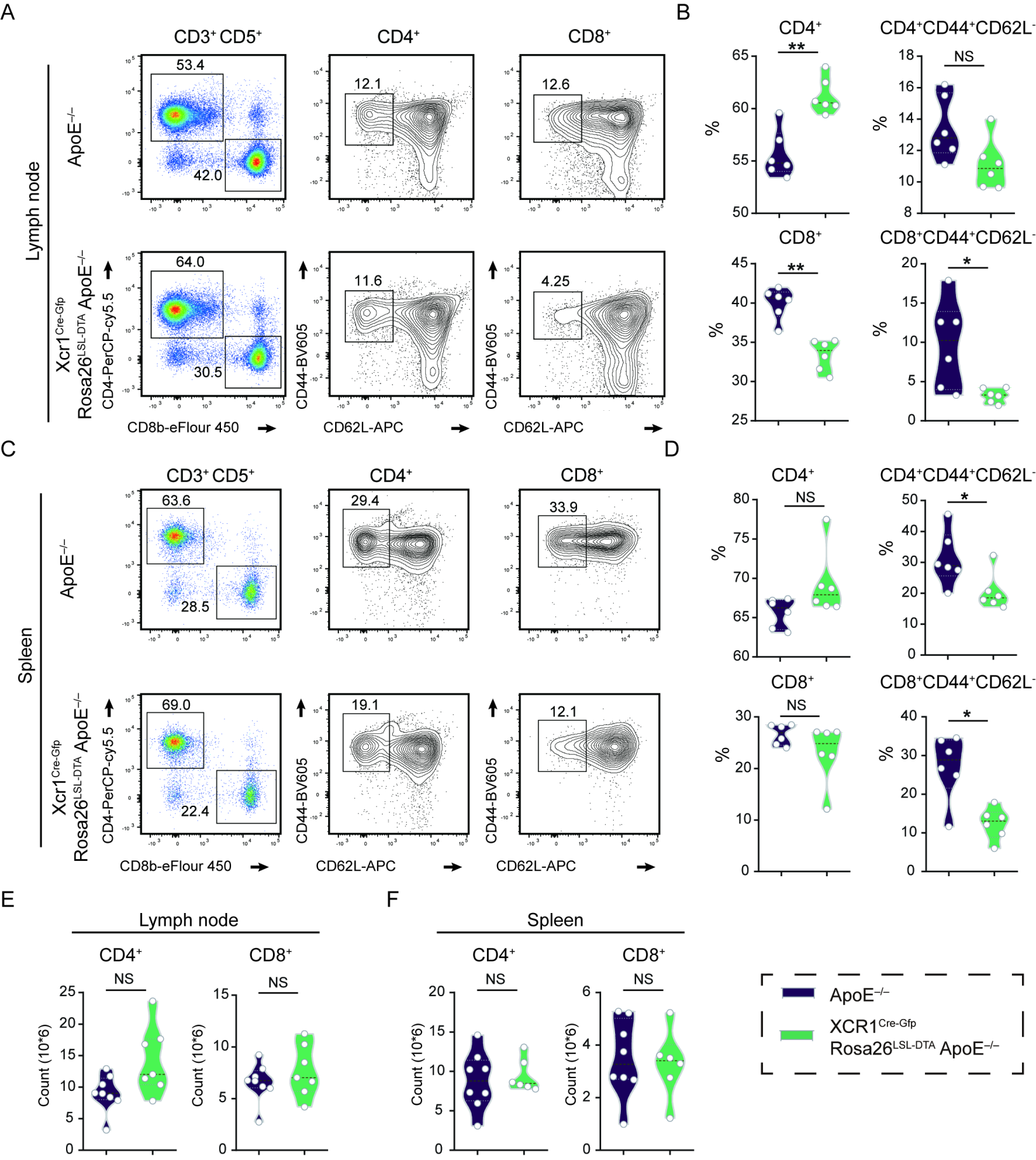
A
Lymph node
ApoE−/−
Xcr1Cre-Gfp Rosa26LSL-DTA ApoE−/−
CD3+ CD5+
CD4+
CD8+
53.4
42.0
12.1
12.6
64.0
30.5
11.6
4.25
CD4-PerCP-cy5.5
CD44-BV605
CD8b-eFlour 450
CD62L-APC
B
CD4+
CD4+CD44+CD62L-
CD8+
CD8+CD44+CD62L-
%
**
NS
*
C
Spleen
63.6
28.5
29.4
33.9
69.0
22.4
19.1
12.1
D
E
Lymph node
Count (10*6)
F
Spleen
ApoE−/−
XCR1Cre-Gfp Rosa26LSL-DTA ApoE−/−

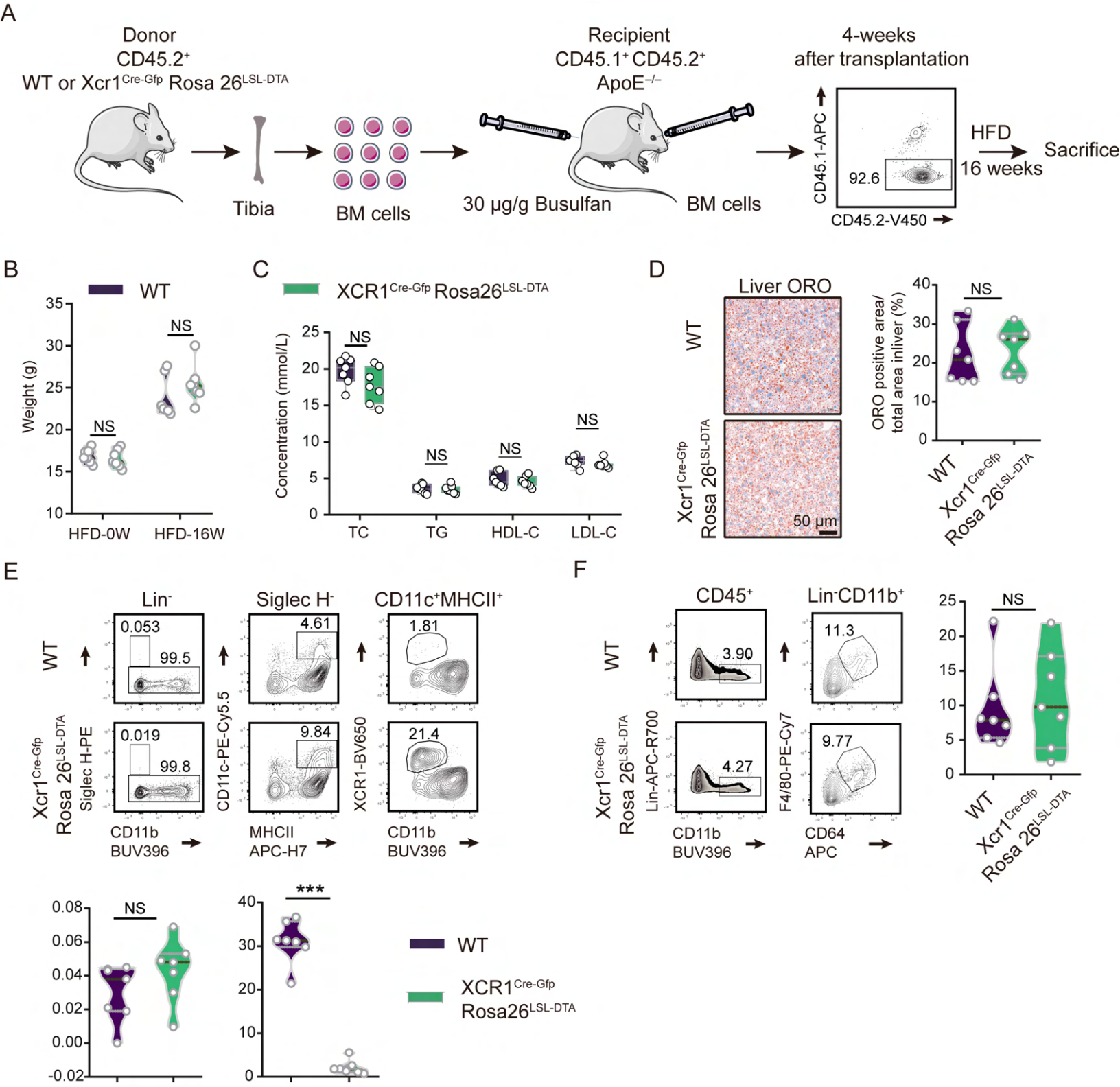
A
Donor
CD45.2+
WT or Xcr1Cre-Gfp Rosa 26LSL-DTA
Tibia
BM cells
Recipient
CD45.1+ CD45.2+
ApoE−/−
30 μg/g Busulfan
BM cells
4-weeks
after transplantation
CD45.1-APC
CD45.2-V450
92.6
HFD
16 weeks
Sacrifice
B
WT
Weight (g)
NS
HFD-0W
HFD-16W
C
XCR1Cre-Gfp Rosa26LSL-DTA
Concentration (mmol/L)
TC
TG
HDL-C
LDL-C
D
Liver ORO
WT
Xcr1Cre-Gfp Rosa 26LSL-DTA
50 μm
ORO positive area/ total area inliver (%)
E
Lin-
Siglec H-
CD11c+MHCII+
0.053
99.5
4.61
1.81
0.019
99.8
9.84
21.4
Siglec H-PE
CD11c-PE-Cy5.5
XCR1-BV650
CD11b BUV396
MHCII APC-H7
F
CD45+
Lin-CD11b+
3.90
11.3
4.27
9.77
Lin-APC-R700
F4/80-PE-Cy7
CD64 APC
***

Single-cell RNA sequencing process

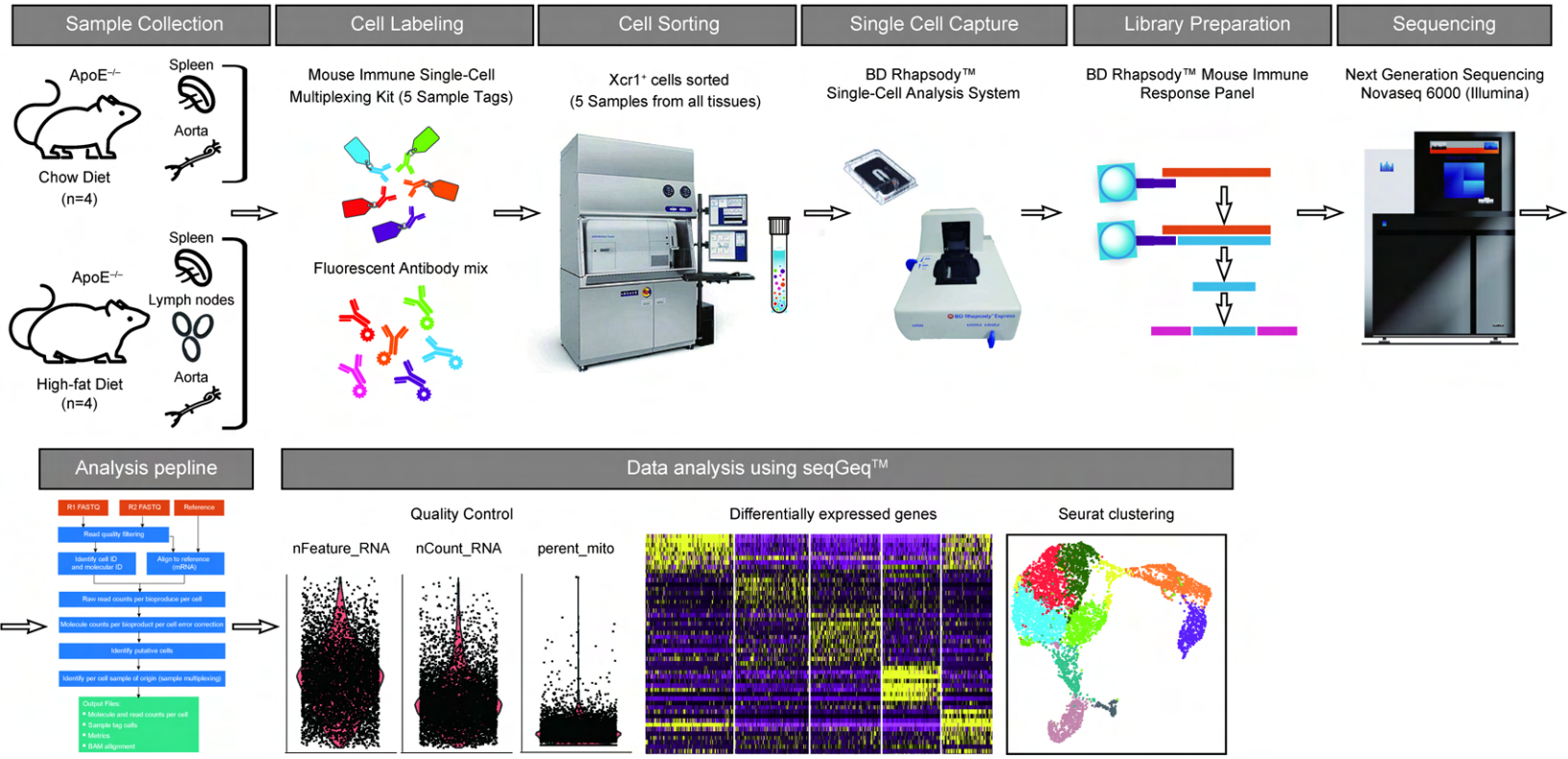

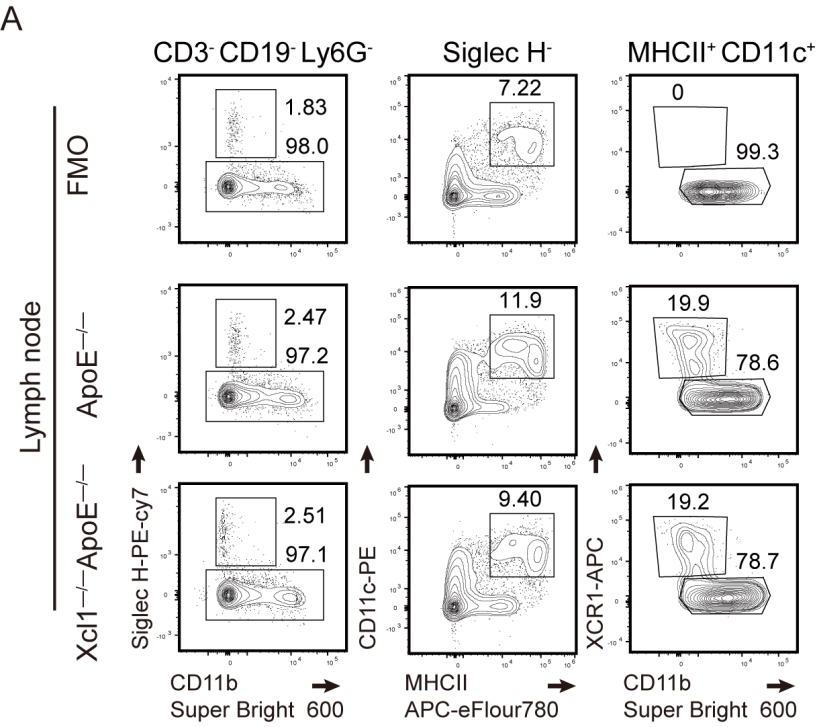
A
CD3- CD19- Ly6G-
Siglec H-
MHCII+ CD11c+
Lymph node
FMO
ApoE−/−
Xcl1−/−ApoE−/−
1.83
98.0
7.22
0
99.3
2.47
97.2
11.9
19.9
78.6
2.51
97.1
9.40
19.2
78.7
Siglec H-PE-cy7
CD11c-PE
XCR1-APC
CD11b Super Bright 600
MHCII APC-eFlour780
CD11b Super Bright 600

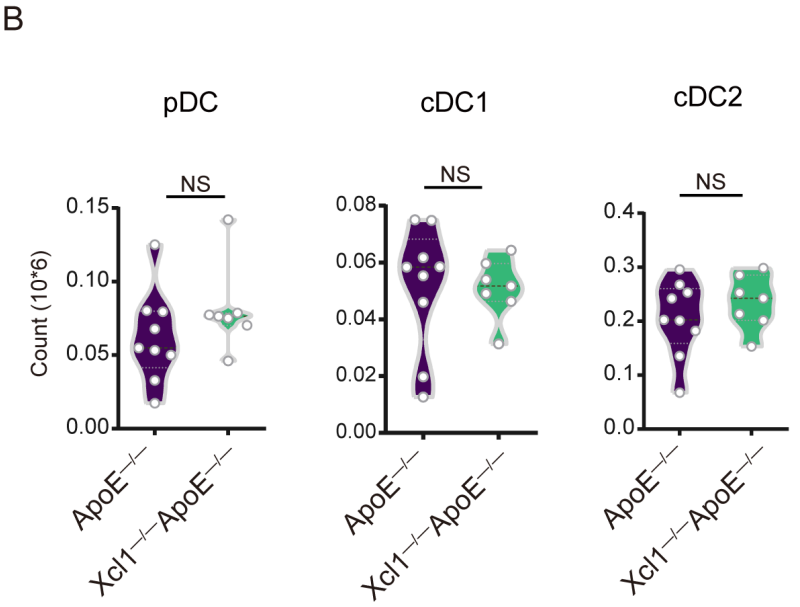
B
pDC
cDC1
cDC2
NS
Count (10*6)
ApoE−/−
Xcl1−/−ApoE−/−

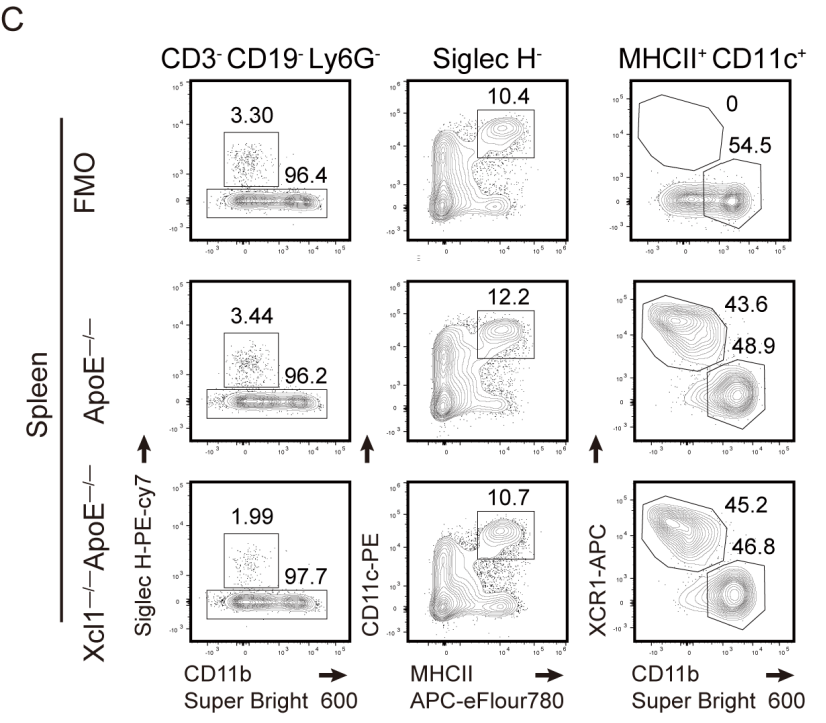
C
CD3- CD19- Ly6G-
Siglec H-
MHCII+ CD11c+
Spleen
FMO
ApoE−/−
Xcl1−/−ApoE−/−
3.30
96.4
10.4
0
54.5
3.44
96.2
12.2
43.6
48.9
1.99
97.7
10.7
45.2
46.8
Siglec H-PE-cy7
CD11c-PE
XCR1-APC
CD11b Super Bright 600
MHCII APC-eFlour780
CD11b Super Bright 600

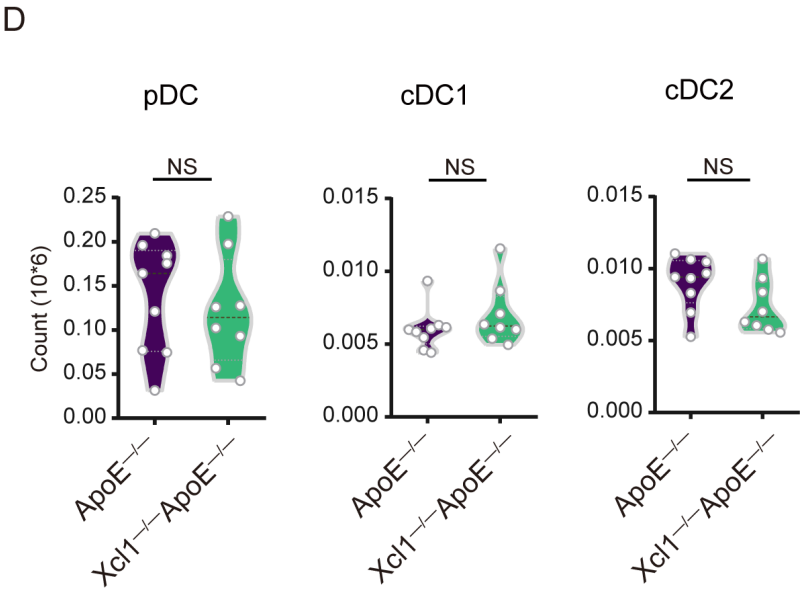
D
pDC
cDC1
cDC2
NS
Count (10*6)
ApoE−/−
Xcl1−/−ApoE−/−

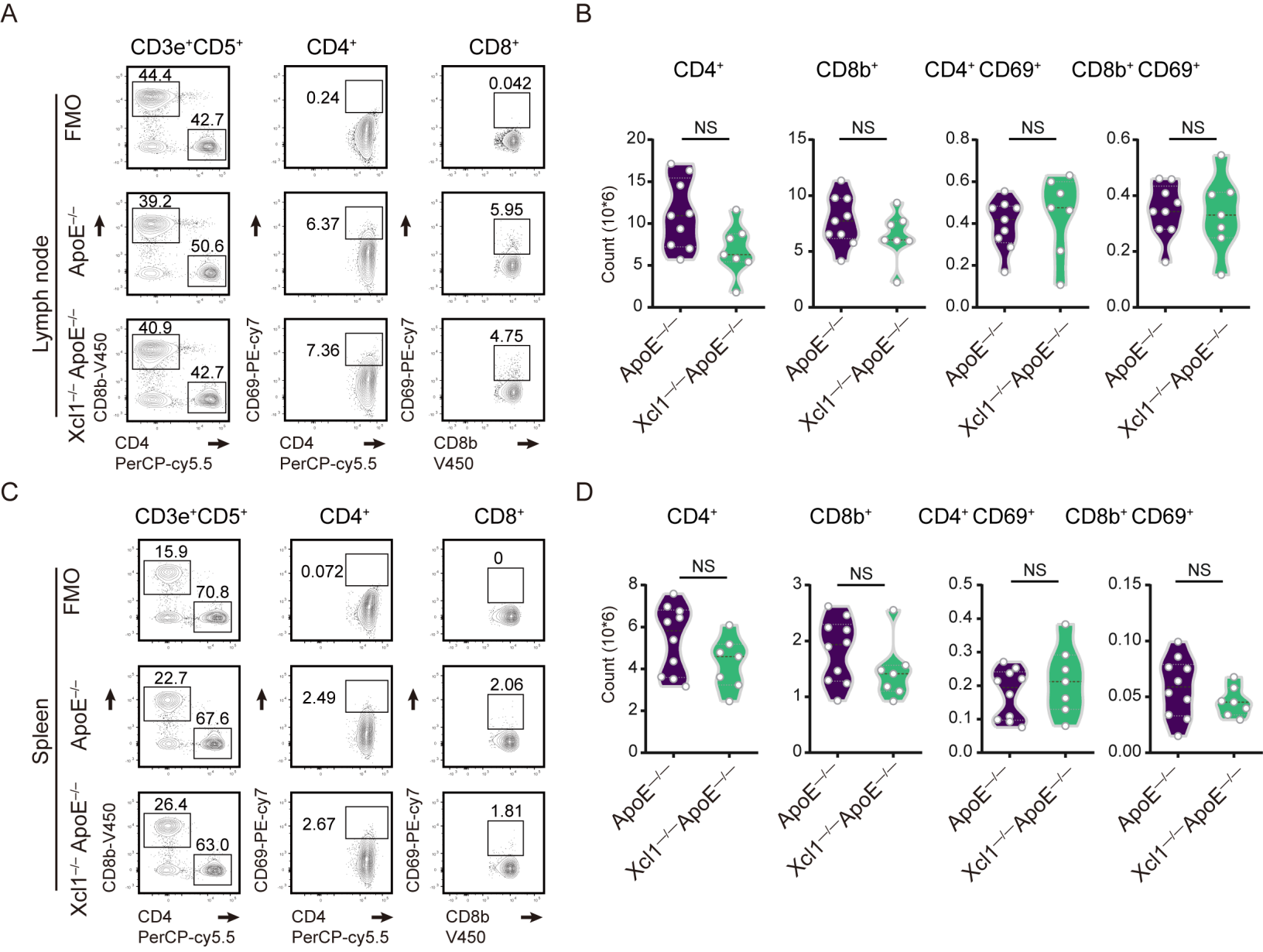
A
CD3e+CD5+
CD4+
CD8+
Lymph node
FMO
ApoE−/−
Xcl1−/− ApoE−/−
44.4
42.7
0.24
0.042
39.2
50.6
6.37
5.95
40.9
42.7
7.36
4.75
CD8b-V450
CD69-PE-cy7
CD69-PE-cy7
CD4
PerCP-cy5.5
CD4
PerCP-cy5.5
CD8b
V450
B
CD4+
CD8b+
CD4+ CD69+
CD8b+ CD69+
NS
Count (10*6)
ApoE−/−
Xcl1−/−ApoE−/−
C
CD3e+CD5+
CD4+
CD8+
Spleen
FMO
ApoE−/−
Xcl1−/− ApoE−/−
15.9
70.8
0.072
0
22.7
67.6
2.49
2.06
26.4
63.0
2.67
1.81
CD8b-V450
CD69-PE-cy7
CD69-PE-cy7
CD4
PerCP-cy5.5
CD4
PerCP-cy5.5
CD8b
V450
D
CD4+
CD8b+
CD4+ CD69+
CD8b+ CD69+
NS
Count (10*6)
ApoE−/−
Xcl1−/−ApoE−/−